Oxysterols Present in Alzheimer's Disease Braininduce Synaptoxicity by Activating Astrocytes: A Major Role for Lipocalin-2

Erica Staurenghi (erica.staurenghi@unito.it)
Department of Clinical and Biological Sciences, University of Turin, Turin, Italy https://orcid.org/0000-0001-5035-7401

Valentina Cerrato
Department of Clinical and Biological Sciences, University of Turin, Turin, Italy

Paola Gamba
Department of Clinical and Biological Sciences, University of Turin, Turin, Italy

Gabriella Testa
Department of Clinical and Biological Sciences, University of Turin, Turin, Italy

Serena Giannelli
Department of Clinical and Biological Sciences, University of Turin, Turin, Italy

Valerio Leoni
Department of Medicine and Surgery, University of Milan-Bicocca, Desio, Monza-Brianza (MB), Ital

Claudio Caccia
Fondazione IRCCS Istituto Neurologico Carlo Besta

Annalisa Buffo
Unit of Medical Genetics and Neurogenetics, Fondazione IRCCS IstitutoNeurologico Carlo Besta, Milan, Italy

Wendy Noble
Institute of Psychiatry, Psychology and Neuroscience, Department of Basic and Clinical Neuroscience, King's College London, London, UK

Beatriz Gomez Perez-Nievas
Institute of Psychiatry, Psychology and Neuroscience, Department of Basic and Clinical Neuroscience, King's College London, London, UK

Gabriella Leonarduzzi
Department of Clinical and Biological Sciences, University of Turin, Turin, Ital

---

Research article

Keywords: Oxysterols, Astrocytes, Astrocyte reactivity, Lipocalin-2, Neurons, Synapses, Synaptotoxicity, Alzheimer's disease

Posted Date: August 14th, 2020

DOI: https://doi.org/10.21203/rs.3.rs-52307/v1

Oxysterols present in Alzheimer's disease brain induce synaptoxicity by activating astrocytes: a major role for lipocalin-2

Erica Staurenghi[1*], Valentina Cerrato[2,3], Paola Gamba[1], Gabriella Testa[1], Serena Giannelli[1], Valerio Leoni[4], Claudio Caccia[5], Annalisa Buffo[2,3], Wendy Noble[6§], Beatriz Gomez Perez-Nievas[6§], Gabriella Leonarduzzi[1§].

[1]*Department of Clinical and Biological Sciences, University of Turin, Turin, Italy.* erica.staurenghi@unito.it, paola.gamba@unito.it, gabriella.testa@unito.it, serena.giannelli@unito.it, gabriella.leonarduzzi@unito.it

[2]*Department of Neuroscience Rita Levi-Montalcini, University of Turin, Turin, Italy.* valentina.cerrato@unito.it, annalisa.buffo@unito.it

[3]*Neuroscience Institute Cavalieri Ottolenghi, Orbassano, Turin, Italy.* valentina.cerrato@unito.it, annalisa.buffo@unito.it

[4]*Department of Medicine and Surgery, University of Milan-Bicocca, Desio, Monza-Brianza (MB), Italy.* valerio.leoni@unimib.it

[5]*Unit of Medical Genetics and Neurogenetics, Fondazione IRCCS Istituto Neurologico Carlo Besta, Milan, Italy.* claudio.caccia@istituto-besta.it

[6]*Institute of Psychiatry, Psychology and Neuroscience, Department of Basic and Clinical Neuroscience, King's College London, London, UK.* wendy.noble@kcl.ac.uk, beatriz.gomez_perez-nievas@kcl.ac.uk

*Corresponding author: Erica Staurenghi erica.staurenghi@unito.it

§ Wendy Noble, Beatriz Gomez Perez-Nievas, and Gabriella Leonarduzzi equally contributed to this work and are joint last authors.

Abstract

Background: Among Alzheimer's disease (AD) brain hallmarks, the presence of reactive astrocytes was demonstrated to correlate with neuronal loss and cognitive deficits. Evidence indeed supports the role of reactive astrocytes as mediators of changes in neurons, including synapses. However, the complexity and the outcomes of astrocyte reactivity are far from being completely elucidated.

Another key role in AD pathogenesis is played by alterations in brain cholesterol metabolism. Oxysterols (cholesterol oxidation products) are crucial for brain cholesterol homeostasis, and we previously demonstrated that changes in the brain levels of various oxysterols correlate with AD progression. Moreover, oxysterols have been shown to contribute to various pathological mechanisms involved in AD pathogenesis.

In order to deepen the role of oxysterols in AD, we investigated whether they could contribute to astrocyte reactivity, and consequently impact on neuronal health.

Methods: Mouse primary astrocyte cultures were used to test the effect of two oxysterol mixtures, that represent the oxysterol composition respectively of mild or severe AD brains, on astrocyte morphology, markers of reactivity, and secretion profile. Co-culture experiments were performed to investigate the impact of oxysterol-treated astrocytes on neurons. Neuronal cultures were exposed to astrocyte conditioned media (ACM) deprived of lipocalin-2 (Lcn2) to investigate the contribution of this mediator to synaptotoxicity.

Results: Results showed that oxysterols induce a clear morphological change in astrocytes, accompanied by the upregulation of some reactive astrocyte markers, including Lcn2. Moreover, ACM analysis revealed a significant increase in the release of Lcn2, cytokines, and chemokines in

response to oxysterols. A significant reduction of postsynaptic density protein 95 (PSD95) and a concurrent increase in cleaved caspase-3 protein levels have been demonstrated in neurons co-cultured with oxysterol-treated astrocytes, pointing out that mediators released by astrocytes have an impact on neurons. Among these mediators, Lcn2 has been demonstrated to play a major role on synapses, affecting neurite morphology and decreasing dendritic spine density.

Conclusions: These data demonstrated that oxysterols present in the AD brain promote astrocyte reactivity, determining the release of several mediators that affect neuronal health and synapses. Lcn2 has been shown to exert a key role in mediating the synaptotoxic effect of oxysterol-treated astrocytes.

Keywords: Oxysterols; Astrocytes; Astrocyte reactivity; Lipocalin-2; Neurons; Synapses; Synaptotoxicity; Alzheimer's disease.

BACKGROUND

Alzheimer's disease (AD) is a neurodegenerative disorder, that represents the most common form of dementia and affects millions of people worldwide [1]. The pathogenic hallmarks of AD are extracellular deposits of amyloid-β (Aβ) peptides in the form of senile plaques and intracellular neurofibrillary tangles (NFTs) made of hyperphosphorylated tau protein. These lesions are typically accompanied by gliosis, especially surrounding senile plaques [2]. Neuronal death and synapse loss are also observed; in particular, synaptic loss exceeds neuronal loss, meaning that remaining neurons also lose synapses. Synapse loss is indeed the best correlate of cognitive decline [3].

Astrocytes play a crucial role in maintaining brain homeostasis and their reaction to different kind of insults leads to a heterogeneous range of changes, known as "astrocyte reactivity" [4]. An increase in the number of reactive astrocytes is a typical histopathological feature of AD brain, and it correlates with cognitive decline and neuronal loss also in transgenic mouse models [5, 6]. Besides

morphological changes and the upregulation of common markers of reactivity (e.g. the glial fibrillary acidic protein, GFAP), reactive astrocytes show significant alterations in gene expression and functions, depending on the specific stimulus [7, 8]. However, the outcome of astrocyte reactivity is still somewhat controversial. Several studies highlighted that reactive astrocytes lose neuroprotective functions, including their ability to promote neurite growth, neuronal survival, and synapse formation [9, 10]. One of the mechanisms through which astrocytes could have an impact on neurons is by the altered release of different kinds of molecules including cytokines, chemokines, growth factors, and neurotransmitters. For instance, an increase in the release of inflammatory mediators by reactive astrocytes has been shown to affect neuronal viability, tau phosphorylation [9, 11], and synaptic function [12, 13]. Another mediator released by reactive astrocytes is lipocalin-2 (Lcn2), a protein identified as a pan-reactive astrocyte marker [8]. Lcn2 is a member of the lipocalin protein family, consisting of more than 20 proteins that transport small hydrophobic molecules (e.g steroids, lipids, and retinoids) and it plays important roles in the immune response, cell migration and proliferation [14]. Increased levels of Lcn2 have been found in the entorhinal cortex and hippocampus of AD brain [15]. Emerging evidence indicates that Lcn2 in the brain is synthethized and secreted as an inducible factor by activated microglia, reactive astrocytes, neurons, and endothelial cells in response to inflammatory stimuli, infections or other insults [16, 17].

In addition to amyloid plaques and NFTs, Alois Alzheimer originally described the presence of “adipose inclusions” in the glial cells of AD brains, suggesting a malfunctioning of lipid metabolism [18]. A clear link between AD and lipid metabolism was established later by the identification of the *ε4* allele of apolipoprotein E (ApoE) as a strong genetic risk factor for AD [19]. Moreover, in the last few decades, much other evidence supports a role for lipids, in particular cholesterol, in AD pathogenesis [20-22]. As the main lipid component of neuronal and glial membranes, as well as a key constituent of myelin, cholesterol plays an essential role in synapse formation, maintenance, and function [23, 24]. Astrocytes are the main producers of cholesterol in

96 the brain, that is delivered to neurons loaded into ApoE-containing lipoproteins. Brain cholesterol
97 homeostasis is closely controlled by pathways regulating cholesterol biosynthesis, storage, and
98 elimination; in particular, the main process responsible for cholesterol elimination is enzymatic
99 oxidation to oxysterols that are able to cross the blood-brain barrier (BBB). Excess brain cholesterol
100 is essentially oxidized to 24-hydroxycholesterol (24-OHC) by cholesterol 24-hydroxylase
101 (CYP46A1), a member of the cytochrome P450 family mainly expressed by neurons; the additional
102 hydroxyl group enables 24-OHC to flow into the circulation crossing the BBB [25]. Smaller amounts
103 of other enzymatic oxysterols, such as 27-hydroxycholesterol (27-OHC), can be produced in the
104 brain, as well as various oxysterols deriving from cholesterol non-enzymatic oxidation mediated by
105 various compounds (e.g. free radical species, metal cations, and Aβ peptides) [26, 27]. Oxysterols are
106 not only cholesterol metabolites but they also play many regulatory functions, such as modulating
107 cholesterol biosynthesis, inflammatory pathways, and the immune response [28]. We have previously
108 demonstrated a correlation between changes in brain levels of various oxysterols and AD progression.
109 Through analysis of the oxysterol composition in AD and aged-matched control cortex, we observed
110 a significant increase in the levels of various enzymatic (e.g. 27-OHC) and non-enzymatic oxysterols
111 (e.g. 7α-hydroxycholesterol, 7α-OHC; 7β-hydroxycholesterol, 7β-OHC; 7-ketocholesterol, 7-KC;
112 5α,6α-epoxycholesterol, α-EPOX; 5β,6β-epoxycholesterol, β-EPOX). In contrast, 24-OHC levels
113 were markedly decreased compared to control brains, probably due to the decline in CYP46A1
114 expression levels as a result of neuronal loss [27]. The effects of oxysterols are still controversial but
115 growing evidence suggests that some of them (e.g. 27-OHC, 7-KC, 7α- and 7β-OHC) may play a
116 role in AD pathogenesis by inducing oxidative stress, inflammation [29], Aβ formation and
117 accumulation [30, 31], tau hyperphosphorylation [32], synaptic dysfunction [33], and cell death [34,
118 35].

119 At present, data regarding the impact of oxysterols on astrocytes are limited and mostly related
120 to the ability of some of them to affect brain cholesterol synthesis and transport in various astrocytic

cell lines [36, 37]. For instance, it has been shown that an increase in systemic levels of 27-OHC can disrupt brain cholesterol homeostasis in rats by reducing cholesterol synthesis and increasing its efflux, but also favouring brain cholesterol accumulation likely due to cell damage; moreover, spatial learning and memory deficits were described as a result [38]. 27-OHC was also observed to induce oxidative stress and to downregulate the antioxidant response in C6 glioma cells, leading to cell toxicity [39]. 24-OHC has been shown to affect redox homeostasis in human glial cells, although its impact may depend on the concentration [40]. Interestingly, the oxysterols 7-KC, 7α-OHC, and 7β-OHC have been shown to inhibit cell growth and decrease viability in several neuronal and glial cell lines; in particular, 7-KC and 7β-OHC exhibited cytotoxic effects also in mixed glial murine primary cultures [35]. High concentrations of 7β-OHC have also been observed to induce toxic effects and morphological changes in an *in vitro* model of reactive astrocytes [41].

Since growing data support the involvement of oxysterols in several aspects of AD pathology and given the presence of reactive astrocytes in the disease, we wanted to investigate whether these compounds could impact on astrocyte reactivity, potentially compromising neuronal health. With the aim of mimicking the human AD brain oxysterol composition, we used two oxysterol mixtures, both including the main seven oxysterols previously quantified in cortical AD brain samples and representative of early or late stages of the disease [27], to investigate the effect of oxysterols in mouse cortical astrocytes and neuronal cultures.

METHODS

Composition of oxysterol mixtures

Cell cultures were treated with two oxysterol mixtures, whose compositions represent oxysterol amounts previously quantified in mild (Early AD mixture) or severe (Late AD mixture) AD brain samples [27]. Both oxysterol mixtures consist of the same seven oxysterols but in different

proportions. Early AD mixture composition: 24-OHC (52.9%), 27-OHC (3%), 7-KC (9.2%), 7α-OHC (4.5%), 7β-OHC (19.2%), α-EPOX (3%), and β-EPOX (8.2%). Late AD mixture composition: 24-OHC (33.4%), 27-OHC (5.8%), 7-KC (12.7%), 7α-OHC (5.4%), 7β-OHC (23.8%), α-EPOX (4.9%), and β-EPOX (14%). Oxysterols were dissolved in absolute ethanol.

Oxysterols were provided as described: 24-OHC (5275, Medical Isotopes, Pehlam, NH, USA), 27-OHC (700061P), 7-KC (700015P), 7α-OHC (700034P), 7β-OHC (700035P) (Avanti Polar Lipids, Alabaster, AL, USA), α-EPOX (C4130-000), and β-EPOX (C5030-000) (Steraloids, Newport, RI, USA).

Primary cultures and co-cultures

Primary astrocyte cultures were obtained from cerebral cortex of wild type CD1 mice on postnatal day 1-3 as previously described [42]. Briefly, after dissociation of the cortices, cells were re-suspended in growing medium (DMEM high glucose with glutaMAX, sodium pyruvate, 10% fetal bovine serum, 100 U/ml penicillin, 100 µg/ml streptomycin) and seeded into T75 flasks, previously coated with poly-D-lysine (10 µg/ml) for at least 1h at 37°C. Astrocytes were cultured for 7-14 days in a humidified 5% CO_2 incubator at 37°C, shaking them at 200 rpm overnight on days 3 and 7 to remove microglia and oligodendrocytes. The absence of microglial contamination was assessed by immunocytochemistry and Western blotting using antibodies that recognize the ionized calcium binding adaptor molecule 1 (Iba1, microglial marker) (Supplemental Fig. 1). Astrocyte-enriched cultures were then re-plated into 12-wells plates using trypsin and the medium was changed to Neurobasal serum-free medium (supplemented with 2% B-27, 2 mM glutaMAX, 100 U/ml penicillin, 100 µg/ml streptomycin) 24h before treatment. Astrocyte cultures were treated with the oxysterol mixtures (Early or Late at different concentrations) up to 24h. Vehicle (ethanol) was added to control astrocytes.

Primary neurons were obtained from cerebral cortex of wild type CD1 mouse embryos at embryonic day 15, according to a previously published protocol [43]. Briefly, after dissociation, cortices were washed twice in HBSS (without Ca^{2+} and Mg^{2+}) and homogenized in 1ml of Neurobasal serum-free medium (supplemented with 2% B-27, 2 mM glutaMAX, 100 U/ml penicillin, 100 µg/ml streptomycin). The suspension was then filtered using a 40 µm cell strainer, live cells were counted and neurons were plated to a density 5×10^5 viable cells per well of 6-wells plates previously coated with poly-D-lysine (10 µg/ml) for at least 1h at 37°C. After 1h, neuron adhesion was checked and the medium was changed. Cultures were maintained at 37°C with 5% CO_2 in Neurobasal serum-free medium. Neuronal cultures were treated at 13-14 days *in vitro* (DIV). For neurite and spine analysis, neurons were transfected at 5-7 DIV with the plasmid peGFP-N1 (Clontech, Mountain View, CA, USA) using Lipofectamine 2000 (Invitrogen, Thermo Fisher Scientific, Waltham, MA, USA) and imaged live 24h after treatment at 14 DIV using an Opera Phenix microscope (Perkin Elmer, Waltham, MA, USA).

For co-culture experiments, primary astrocytes were plated into cell-culture inserts (0.4 µm pore membrane, Falcon, Corning, Corning, NY, USA), that allow the passage of small molecules in culture medium. Astrocytes were pre-treated with the Late AD mixture (10 µM) or vehicle (ethanol) for 12h, medium was changed to remove oxysterols, and inserts on which astrocytes were grown were added to neuron cultures for a further 24h.

Cytotoxicity assay

Cytotoxicity was assessed by measuring levels of lactate dehydrogenase (LDH) enzyme release into the media using Pierce LDH Cytotoxicity Assay Kit (Fisher Scientific, Thermo Fisher Scientific) according to the manufacturers' instructions. Some cells were lysed with 0.5% Triton X-100 and LDH content in the medium was measured in order to evaluate the maximum LDH amount released from dead cells. LDH release was calculated as a percentage of total LDH released by lysed cells.

Gel electrophoresis and Western blotting

After treatments, the cell culture media were collected, cells were washed with PBS and directly lysed with PBS containing sample buffer (NuPAGE LDS Sample Buffer 4X, Invitrogen), reducing agent (NuPAGE Sample Reducing Agent 10X, Invitrogen), protease inhibitor (complete Mini EDTA-Free Protease Inhibitor Cocktail, Roche, Basel, CH) and phosphatase inhibitor (PhosSTOP, Roche) cocktails.

Equal amounts of protein samples (20 µg) were boiled, separated by electrophoresis using 10% precast gels (NuPAGE 10% Bis-Tris Protein Gels, Invitrogen) and then transferred to nitrocellulose membranes (Amersham Protran, GE Healthcare, Chicago, IL, USA). After blocking with Odyssey Blocking Buffer (LI-COR Biosciences, Lincoln, NE, USA) for 1h at room temperature, membranes were incubated with primary antibodies overnight at 4°C. The following primary antibodies were used: GFAP (Z0334, Dako, Agilent Technologies, Santa Clara, CA, USA), Lipocalin-2/NGAL (AF1857, R&D Systems, Minneapolis, MN, USA), SerpinA3N (AF4709, R&D Systems), cleaved caspase-3 (Asp175, 9661, Cell Signaling, Danvers, MA, USA), PSD95 (D74D3, Cell Signaling), Synapsin (6008-30, BioVision, Milpitas, CA, USA), Iba1 (019-19741, Wako Chemicals, Richmond, VA, USA) and β-actin (ab8226, Abcam, Cambridge, UK). After washing to remove unbound antibody with TBS-Tween20 0.05%, the appropriate fluorophore-coupled secondary antibody (1:10000, LI-COR Biosciences) was added for 1h at room temperature. Membranes were washed with TBS-Tween20 0.05% and scanned using an Odyssey infrared imaging system (LI-COR Biosciences). Band intensities were quantified using the Image Studio Software (LI-COR Biosciences) and normalized to the corresponding β-actin bands.

Similarly, to detect secreted Lcn2, 250 µl of culture media were concentrated using centrifugal filters (Amicon Ultra, Millipore, Merck, Darmstadt, DE); the protein concentration was calculated

using the Bradford Assay (Protein Assay Dye Reagent Concentrate, Bio-Rad Laboratories, Hercules, CA, USA), and samples were prepared as above to perform Western blotting of cell culture media.

Immunocytochemistry

Astrocytes were plated on coverslips (12 or 18 mm diameter, No. 1.5) into 12- or 24-wells plates. After treatment, cells were washed with PBS, fixed in 4% paraformaldehyde in PBS for 10 min at room temperature, and then washed again twice with PBS. Cells were permeabilized and blocked (4% goat serum, 0.1% Triton in PBS) for 1h at room temperature before incubating with the anti-GFAP (Z0334, Dako) and/or Iba1 (ab48004, Abcam) primary antibodies (4% goat serum in PBS) overnight at 4°C. The following day, cells were incubated with the appropriate secondary antibody conjugated with fluorescent probes for 1h at room temperature (Alexa Fluor 488 or 594, Invitrogen) and nuclei were stained with Hoescht 33258 (10 µg/ml in PBS, Sigma-Aldrich, St. Louis, MO, USA). Cells were imaged using an Eclipse Ti-E inverted Microscope (Nikon, Tokyo, JP) or LSM800 confocal microscope (Carl Zeiss, Oberkochen, DE).

Cytokine array

Astrocyte culture media was collected and stored at -20°C prior to analysis of cytokine and chemokine content using Mouse Proteome Profiler arrays (Mouse Cytokine Array Panel A, R&D Systems), according to the manufacturers' instructions. Briefly, array membranes were incubated in blocking buffer for 1h at room temperature. Each sample of medium was incubated with the Detection Antibody Cocktail and this mix was then placed onto blocked membranes overnight at 4°C. After washes, membranes were incubated with IRDye 800CW Streptavidin (1:2000, LI-COR Biosciences) for 30 min at room temperature. Membranes were then scanned using an Odyssey infrared imaging system and the spot intensities were quantified using the Image Studio Software (LI-COR

242 Biosciences). Positive and negative control spots included in each membrane allowed quantitative
243 analysis by densitometry and results were expressed as percentage change compared to control
244 cultures.

245

246 **Oxysterol quantification in astrocyte culture medium**

247 Astrocyte culture media (100 µl) was added to a screw-capped vial sealed with a Teflon septum
248 together with D7-7α-hydroxycholesterol (50 ng), D7-7β-hydroxycholesterol (50 ng), D7-7-oxo-
249 cholesterol (50 ng), D6-5α-6α-epoxicholesterol (50 ng), D6-5β-6β-epoxicholesterol, D6-24-
250 hydroxycholesterol (250 ng), D6-27-hydroxycholesterol (50 ng) as internal standards, as well as 50
251 µl of butylated hydroxytoluene (5g/l) and 50 µl of K3-EDTA (10 g/l) to prevent auto-oxidation. Each
252 vial was then flushed with argon for 5 min to remove air. Alkaline hydrolysis, sterol extraction, and
253 gas chromatography-mass spectrometry (GC-MS) analysis were performed as previously described
254 [44].

255

256 **RNA extraction and real-time RT-PCR**

257 Total RNA was extracted using TriFast reagent (Eurogold TriFast, EuroClone, Pero, IT) following
258 the manufacturers' instructions. RNA was dissolved in RNase-free water with RNase inhibitors
259 (SUPERase-In RNase inhibitor, Invitrogen). The amount and purity of the extracted RNA were
260 assessed by using a NanoDrop ND-1000 spectrophotometer (Thermo Fisher Scientific). cDNA was
261 synthesized by reverse transcription of 1 µg of RNA by using a commercial kit and random primers
262 (High-Capacity cDNA Reverse Transcription Kit, Applied Biosystems, Thermo Fisher Scientific)
263 following the manufacturers' instructions.

264 Singleplex real-time RT-PCR was performed on 30 ng of cDNA by using TaqMan Gene
265 Expression Assays for mouse Lcn2 (Mm01324470_m1) and β-actin (Mm02619580_g1), TaqMan

Fast Universal PCR Master Mix, and a 7500 Fast Real-Time PCR System (Applied Biosystems). The PCR cycling parameters were set up as previously described [31]. The fractional cycle number (Ct) was determined for each gene considered and results were then normalized to β-actin expression. Relative quantification of target gene expression was achieved with a mathematical method [45].

Transient gene knockdown

The transient knockdown of Lcn2 gene was performed by using a Small Interfering RNA (siRNA) (Silencer Select Pre-designed siRNA S69122, Ambion, Thermo Fisher Scientific) following the manufacturers' instructions. A non-targeting siRNA was used as a negative control (Silencer Select Negative Control #2 siRNA, Ambion). Briefly, astrocytes were plated into 12- or 24-wells plates and respectively 50 µl or 100 µl of a mix containing siRNA and transfection agent (Lipofectamine RNAiMAX Reagent, Invitrogen) in a 1:1 ratio was added to each well, in order to reach a final siRNA concentration of 100 nM and 3 µl/ml of transfection agent. After 6h transfection, the medium was changed and astrocytes were treated with the Late AD mixture (10 µM) for 12h. After treatment, cells were washed with PBS and fresh medium was added. Astrocyte conditioned media were then collected after another 24h. Protein and RNA extraction, as well as real-time RT-PCR, were performed as described above. The silencing efficiency, validated by real-time RT-PCR, was approximately 85% (Supplemental Fig. 2).

Analysis of neuronal morphology

The neuronal morphology of 14 DIV neurons previously transfected with the plasmid peGFP-N1 (Clontech) on 5-7 DIV and treated on 13 DIV was assessed using high resolution digital images of live neurons taken using an Opera-Phenix microscope (Perkin-Elmer). Neurite complexity was analysed using Harmony software: total and maximum neurite length, and number of nodes and

extremities were quantified and compared between groups. NeuronStudio software (CNIC, Mount Sinai School of Medicine) was used for dendritic spine analysis. Spine density was defined as number of spines per micrometer of dendrite length. Dendritic spine densities were calculated from 20 neurons/condition.

Statistical analysis

After performing a Shapiro-Wilk normality test, data were analysed using one-way ANOVA followed by Bonferroni *post hoc* test or Student's t-test (GraphPad Prism 7 Software, Graphpad Software, La Jolla, CA, USA). Results were considered statistically significant when $P<0.05$. Data are represented as means ± standard deviation.

RESULTS

Oxysterol mixtures induce a morphological change in astrocytes

Astrocyte reaction to certain stimuli is defined by a wide range of heterogeneous responses, including changes in morphology [7, 46]. To analyse the effect of oxysterols on astrocyte morphology and survival, cells were exposed to increasing concentrations of the Early and Late mixtures (1, 5 or 10 µM). Exposure of primary astrocytes to 5 or 10 µM of both oxysterol mixtures for 24h induced a clear change in their morphology with astrocytes adopting a more stellate "brain-like" and reactive appearance rather than the large, flat fibroblast-like morphology typical of unstimulated dissociated astrocytes in culture (Fig. 1B). Importantly, this was not accompanied by cell death since there were no significant increases in the abundance of LDH released into culture medium following treatment when compared to control cultures (Fig. 1A). Time course treatments showed that astrocytes started to display the typical signs of reactivity (increase in the number of GFAP positive processes and

stellate appearance) after 12h of exposure to 10 μM of both Early and Late mixtures, with these changes becoming more evident 24h after treatment (Fig. 2).

Oxysterol mixtures increase the synthesis of the pan-reactive astrocyte markers Lcn2 and SerpinA3N

To validate the induction of astrocytic reactivity by oxysterols, and to confirm that the morphological alteration is accompanied by functional changes, we determined whether treatment with the Early or Late AD mixtures led to an increase in the levels of some pan-reactive astrocyte markers [8]. Exposure to both oxysterol mixtures (10 μM) resulted in a marked increase in Lcn2 and serine protease inhibitor A3N (SerpinA3N) protein levels at 12h ($P<0.0001$ and $P<0.001$) and 24h ($P<0.0001$) (Fig. 3), contemporaneous with morphological changes. These molecules are involved in the acute-phase response and were both identified as new reactive astrocyte markers [8, 47]. Total levels of GFAP were only slightly increased ($P<0.05$) or remained unchanged in response to the mixtures (Fig. 3), suggesting that the observed morphological changes are not only dependent on the expression of GFAP.

Oxysterol-induced reactivity triggers the release of Lcn2, cytokines, and chemokines by astrocytes

Astrocyte reactivity is typically characterized by the release of cytokines, chemokines, and other mediators, that could have several effects on the surrounding cells [48]. Therefore, we investigated whether oxysterol-mediated astrocyte reactivity was accompanied by altered release of mediators into the cell culture medium.

Since Lcn2 is secreted by reactive astrocytes [17, 49], we analysed its protein levels in astrocyte conditioned media (ACM) by Western blotting. We saw that the robust increase in

intracellular levels of Lcn2 is accompanied by a significant increase in the secretion of Lcn2 after 24h treatment with 10 μM of both Early and Late oxysterol mixtures ($P<0.0001$) (Fig. 4A).

The amounts of 40 cytokines and chemokines in ACM samples were next evaluated using Proteome Profiler antibody arrays. The analysis showed a significant increase in the release of several mediators by astrocytes treated for 24h, especially with the Late AD oxysterol mixture (10 μM). Some of the cytokines found to be increased in the medium of astrocytes treated with this oxysterol mixture were interleukin-1β (IL-1β), soluble intercellular adhesion molecule-1 (sICAM-1) ($P<0.001$), IL-1α, IL-5, granulocyte colony-stimulating factor (G-CSF), and C-C motif chemokine 12 (CCL12) ($P<0.01$). In addition, the levels of CCL1, IL-7, IL-10, IL-13, IL-16, IL-17, and C-X-C motif chemokine 9 (CXCL9) were slightly but significantly increased compared to levels in control media ($P<0.05$) (Fig. 4B, C). In contrast, when astrocytes were exposed to the Early AD oxysterol mixture (10 μM), only sICAM-1 ($P<0.01$), IL-1α, and IL-1β ($P<0.05$) were found to be significantly increased relative to levels in control ACM, highlighting a different impact of the two oxysterol mixtures on astrocyte cytokine and chemokine release (Fig. 4C).

Oxysterol-stimulated astrocytes compromise neuronal health

It has previously been shown that astrocyte reactivity depends on the specific stimulus and that heterogeneous responses of reactive astrocytes involves different signaling pathways. The consequences of these alterations for astrocytic support of neuronal health requires further investigation [7, 47].

To test the effect of oxysterol-stimulated astrocytes on neuronal health, we performed co-culture experiments. GC-MS analysis of oxysterols in ACM showed that, although variable, a substantial proportion (8-54%) of some oxysterols remain in ACM 24h after treatment (Supplemental Fig. 3). Since these oxysterols are known to directly affect neuron viability [31, 33, 50], we co-

362 cultured neurons with astrocytes that had been pre-treated with oxysterols. As shown in Figure 5A,
363 astrocytes grown on cell culture inserts were pre-treated for 12h with the Late AD oxysterol mixture
364 (10 μM) and then transferred to culture plates containing neurons for a further 24h: this allowed us
365 to investigate the effect of mediators released from stimulated astrocyte on neurons, without
366 transferring oxysterols that remained in ACM. In parallel, neuronal cultures were treated with the
367 Late AD mixture or with ethanol for 24h in the absence of astrocytes, in order to assess the direct
368 effect of the same oxysterol mixture on neurons.

369 Interestingly, Western blotting analysis showed a significant reduction of postsynaptic density
370 protein 95 (PSD95) levels ($P<0.05$), a scaffold protein important for postsynaptic density structure
371 and function, in neurons cultured with astrocytes that had been previously exposed to oxysterols (Fig.
372 5B). This reduction was accompanied by a significant increase in the amount of cleaved (active)
373 caspase-3 ($P<0.01$) (Fig. 5B), that was demonstrated to play various non-apoptotic roles in neurons
374 including to affect synaptic functions [51]. A mild but not significant reduction of the pre-synaptic
375 marker synapsin was also observed. Moreover, when neurons were directly treated with oxysterols,
376 PSD95 ($P<0.05$), cleaved caspase-3 ($P<0.01$), and synapsin levels ($P<0.05$) were all significantly
377 altered (Fig. 5B), confirming previous results showing that oxysterols directly compromise neuron
378 health [31, 33]. Importantly, all these results were obtained in the absence of significant neuronal
379 death, as assessed by LDH release (Supplemental Fig. 4). Overall, these data suggest that factors
380 released by astrocytes in response to the oxysterol mixture, whose composition is similar to AD brain
381 oxysterol content, compromise synaptic and neuronal health without causing overt neurotoxicity.

382

383 **Lcn2 secreted by oxysterol-stimulated astrocytes affects neurite complexity and decreases**
384 **dendritic spine density**

Lcn2 has previously been shown to affect synapses, neuronal health and morphology, [17, 52, 53]. To investigate whether Lcn2 could play a role in mediating the effect of oxysterol-stimulated astrocytes on neurons, Lcn2 expression was silenced in astrocytes prior to determining the impact of ACM on neuron morphology. To further investigate the effects of ACM on synapses under these conditions, dendritic spine density was also evaluated.

For this purpose, astrocytes were transfected for 6h with Lcn2 or scrambled siRNA, and the medium removed prior to treatment with the Late AD mixture (10 μM) for 12h. The medium was removed and fresh medium was added for another 24h, to obtain ACM without oxysterols. Both real-time RT-PCR (Fig. 6A) and Western blotting results (Fig. 6B) confirmed that siRNA-mediated Lcn2 gene silencing prevents the increase in Lcn2 expression, synthesis, and release into the medium induced by the Late AD oxysterol mixture, compared to control conditions (scrambled siRNA). Interestingly, oxysterol-induced morphological changes were not prevented by Lcn2 gene silencing, suggesting that the pathway by which oxysterols induce astrocyte alterations is not dependent upon the presence of Lcn2 (Fig. 6C).

Next, ACM was added to cultured neurons to determine the impact of secreted Lcn2 on neuron morphology and dendritic spines. Medium from oxysterol-activated astrocytes transfected with the scrambled siRNA compromises neurite complexity, as shown by reduction of total and maximum neurite length, and the number of nodes, automatically identified by Harmony software ($P<0.05$) (Fig. 7A). Importantly, the addition of ACM was also found to substantially reduce dendritic spine density ($P<0.001$) (Fig. 7B), further indicating a synaptotoxic effect of proteins secreted by oxysterol-stimulated astrocytes. All of these effects were prevented by silencing Lcn2, confirming a key role of Lcn2 in mediating the impact of oxysterol-stimulated astrocytes on neurite complexity and synaptic health (Fig. 7).

DISCUSSION

The pathophysiology of AD is still not fully understood, but evidence supports the involvement of many factors in sporadic AD onset, including inflammation and impaired cholesterol metabolism [54]. Microglia and astrocytes play a role in the neuroinflammation observed in AD and they are found in their activated state in affected brain regions, particularly surrounding amyloid plaques. Astrocyte reactivity is not an exclusive feature of AD brain but the association of reactive astrocytes with amyloid plaques is considered functionally significant. Indeed, post-mortem neuropathological studies have shown that the number of reactive astrocytes increases with disease progression [6, 55], and activated astrocytes and microglia correlate with dementia in AD [5].

Astrocyte reactivity leads to a heterogeneous range of phenotypic, transcriptomic, and functional changes, depending on the specific environmental stimulus [7, 8], including those related to ageing and disease [10, 56]. Here, we observed that application of various oxysterols, in the same proportions as those identified in early and late-stage AD brain, distinctly altered astrocyte morphology after 24h treatment. In particular, astrocytes adopted a more stellate appearance with many long and branched processes evident. In support of these data, 7β-OHC has previously been shown to induce morphological changes, characterized by process elongation, in cultured reactive astrocytes [41]. An increase in the number of processes is considered a reliable feature of reactivity, demonstrated in several cell culture models of reactive astrocytes [57, 58].

Reactive astrocytes were conventionally identified by GFAP immunoreactivity; however, it is noteworthy that different stimuli can lead to similar degrees of GFAP upregulation while causing substantially different changes in transcriptome profile and cell functions [7]. Furthermore, unlike brain astrocytes, most astrocytes in culture are GFAP reactive as a result of the *in vitro* conditions, the absence of their usual environment, and loss of inhibitory influences of neurons [41]. Astrocytes treated with Early or Late AD oxysterol mixtures up to 24h showed a significant but mild increase in GFAP protein levels despite the extensive morphological changes

observed. The morphological changes we observed in response to oxysterol mixtures were, however, accompanied by a marked upregulation of Lcn2 and SerpinA3N, both proteins identified as "pan reactive" astrocytes markers [8], as well as by increased release of Lcn2 into culture medium. Lcn2, also known as neutrophil gelatinase-associated lipocalin (NGAL), is an acute phase protein with several roles [14] that is secreted by different kind of cells, including reactive astrocytes [16, 17]. It can act as an autocrine mediator of reactive astrogliosis, since it is able to induce morphological changes in primary astrocytes [57]. In addition, several studies showed that Lcn2 exerts synaptotoxic and neurotoxic effects, affecting neuronal viability, dendritic spine density and morphology, and ultimately cognitive functions [17, 49, 52, 53]. SerpinA3N, also known as alpha1-antichymotrypsin, is a protease inhibitor involved in the acute phase response, that is produced in various tissues including the brain, with reactive and aging astrocytes being the main producers of Lcn2 in the brain [8, 56]. Immunohistochemical analysis of AD brain samples showed that SerpinA3N co-localizes with amyloid plaques, reactive microglia and astrocytes [59]. Moreover, an increase in tau phosphorylation has been observed both in mice overexpressing SerpinA3N and in primary neurons treated with recombinant Lcn2, the latter also showing neurite degeneration and apoptosis [60].

It is well known that in many cases astrocyte activation is accompanied by an increase in the release of several soluble factors, including reactive oxygen species and cytokines [11, 48]. Interestingly, 7α,25-dihydroxycholesterol has been shown to inhibit the lipopolysaccharide (LPS)-induced release of pro-inflammatory cytokines including IL-17/tumor necrosis factor-α (TNF-α) in cultured human astrocytes [61]. Other oxysterols (e.g. 27-OHC) have been demonstrated to decrease LPS-induced expression of IL-6 and TNF-α mRNA in mouse primary glial cells [62]. However, there are no data on how oxysterols directly affect astrocyte secretion profile. Our cytokine array analysis showed that oxysterol treatment significantly increases the release of a wide range of cytokines and chemokines from primary astrocytes after 24h. Interestingly, this analysis highlighted a differential impact of the two oxysterol mixtures: the majority of the significant increases were observed in ACM

459 from astrocytes treated with the mixture that mimics late AD brain composition. Among the released
460 mediators, inflammatory cytokines (IL-1α, IL-1β, and IL-17), adhesion molecules (sICAM-1),
461 growth factors and chemokines (IL-5, IL-7, IL-16, G-CSF, CCL1, CCL12, and CXCL9),
462 immunoregulatory cytokines (IL-5 and IL-13), and anti-inflammatory cytokines (IL-10) were
463 elevated. In particular, IL-1β and sICAM-1 were the most significantly increased. Astrocytes are both
464 targets and effectors of cytokines and many other mediators that affect not only their immune and
465 inflammatory cell functions but also their synapse-directed and neuronal functions [48]. IL-1β has
466 been previously shown to induce reactive astrogliosis [10], to be released by reactive astrocytes and
467 astrocytes from 5xFAD AD mouse model [63, 64], and to contribute to astrocyte-mediated neuronal
468 death [65]; moreover, its levels are increased in AD brains [27, 66].

469 Using gene ontology classification, proteins involved in extracellular matrix modification and
470 adhesion were identified as the gene class most represented in the transcriptome of reactive astrocytes
471 [8]. ICAM-1 is a transmembrane glycoprotein belonging to the immunoglobulin family of adhesion
472 molecules, expressed not only by endothelial and immune system cells [67] but also by astrocytes
473 [8]. sICAM-1 is released by proteolytic cleavage of the transmembrane protein [64, 68]. Several
474 studies have shown that the addition of sICAM-1 to different *in vitro* models activates pro-
475 inflammatory cascades, including in astrocytes, and inflammatory mediators can in turn favour its
476 release [69, 70]. Furthermore, sICAM-1 levels are increased in AD cerebrospinal fluid and correlate
477 with various AD markers including total tau, phosphorylated tau, and cortical thinning [71, 72]. The
478 data presented here provide the first evidence for a direct impact of oxysterols on astrocyte
479 morphology, markers of reactivity, and secretion profile, and strongly suggest that oxysterol mixtures
480 that mimic oxysterol composition in AD brain induce astrocyte reactivity.

481 The functional implications of astrocyte reactivity are various and very context-dependent.
482 For instance, astrocytes have been shown to mediate Aβ-induced neurotoxicity and tau
483 phosphorylation, as well as to induce a decrease of synaptic markers; interestingly, the release of pro-

484 inflammatory cytokines from astrocytes seems to play a key role in some of these processes [11, 73].
485 To investigate the consequences of oxysterol-mediated astrocytic reactivity on neurons, we exposed
486 neurons to astrocytes that had previously been challenged with oxysterols. Our data indicated that
487 neurons co-cultured with pre-treated astrocytes are characterized by a significant reduction in PSD95
488 protein levels and a clear increase in cleaved caspase-3 protein levels, suggesting that oxysterol-
489 induced reactivity is detrimental for neuronal health. Importantly, similar changes were obtained
490 when neuronal cultures were directly treated with the Late AD mixture in the absence of astrocytes,
491 confirming that oxysterols have a direct and negative effect on neuron health. PSD95 is a scaffold
492 protein abundant in the postsynaptic density (PSD), that anchors N-methyl-D-aspartate receptor
493 (NMDAR) as well as other proteins (e.g potassium channels, cell adhesion molecules) to the PSD. It
494 is also involved in the assembly of specific signaling proteins, that act downstream of NMDAR [74].
495 PSD95 is recognized to play an important role in synaptic plasticity and memory, and in-keeping with
496 this its levels decrease in AD [5]. To the best of our knowledge, no studies have yet assessed the
497 specific actions of oxysterol-treated astrocytes on PSD95 levels, however various mediators released
498 by oxysterol-treated astrocytes have previously been shown to affect synapses, including Lcn2 and
499 IL-1α/β [52, 75, 76]. Indeed, the binding of cytokines and chemokines to their receptors leads to the
500 activation of diverse signaling pathways [77], some of which are involved in PSD95 regulation [78].
501 Concerning oxysterols, it has been demonstrated that 27-OHC reduces dendritic spine density and
502 PSD95 levels in primary mouse hippocampal neurons [33], whereas 24-OHC affects synaptic
503 plasticity via modulation of NMDAR [79]. Since oxysterols are able to directly modulate several
504 pathways involved in PSD95 regulation [50], other oxysterols present into the mixture could be
505 involved in the observed PSD95 reduction, even if their role needs further investigation. Moreover,
506 the ability of oxysterols to alter membrane structure could affect transmembrane protein localization
507 and function, thus modifying the integrity of the PSD structure [80, 81]. The increase in the levels of
508 cleaved caspase-3 fragment further indicates that oxysterol-activated astrocytes are detrimental to
509 neurons. Besides being an effector of apoptosis, caspase-3 was demonstrated to play various non-

apoptotic roles in neurons involved in both physiological processes and neurodegenerative diseases [51]. For instance, it is involved in the pathological cleavage of tau protein [82] and its activation correlates with dendritic spine loss and cognitive decline in the absence of neuronal cell death [83]. Interestingly, it has previously been shown that increase in neuronal cleaved caspase-3 levels in response to Aβ is exacerbated in the presence of reactive astrocytes, and that increased caspase-3 activity is reduced upon pretreatment with an anti-inflammatory molecule *in vitro* [11] and *in vivo* [84]. These and other data highlight that neuronal caspase-3 can be activated by extracellular inflammatory mediators. Caspase-3 can also be activated by oxysterols, mainly those oxidized at C7 position but also others [33, 50, 85-87].

In AD, synaptic loss is the parameter that best correlates with dementia [88, 89]; therefore, elucidating how synapses are lost is of great importance. This can be examined *in vitro* by monitoring dendritic spine density and/or neurite complexity. The direct effect of oxysterols on synaptic health has been partially investigated as stated above, but we were interested in assessing how oxysterol-activated astrocytes affect synapses. Our results indicate that ACM from oxysterol-activated astrocytes is synaptotoxic, as shown by significant decreases in the number of dendritic spines and reduced complexity of the neurites in primary neurons, as well as by PSD95 reduction as described above. Because Lcn2 is secreted upon oxysterol-induced astrocyte activation and has proven to be neurotoxic [17, 53], we tested whether we could revert the synaptotoxic effect of reactive astrocytes by suppressing Lcn2 expression and therefore reducing its secretion. Our results clearly demonstrate that dendritic spine density and neurites architecture are better preserved when Lcn2 expression is silenced prior to treating astrocytes with oxysterols. These data reveal a major role for Lcn2 in mediating the synaptotoxic effect of oxysterol-treated astrocytes. These findings extend previous studies showing that Lcn2 affects dendritic spine density and morphology [52], as well as contributing to hippocampal damage and cognitive impairment in a mouse model of vascular dementia [49].

CONCLUSIONS

Overall, these results describe the complexity of oxysterol effects on astrocytes and neurons. Of interest was our observation that astrocytes respond most strongly to oxysterol mixture representative of late AD brain in comparison to early AD-mimicking mixture. These data add to an emerging consensus that astrocyte responses are differentially altered at specific disease stages in response to various changes in the local environment. Indeed, we demonstrated that oxysterols induce a clear morphological change in astrocytes, that is accompanied by an increase in some reactive astrocyte markers and the release of several mediators. We also demonstrated that oxysterols are detrimental to neuronal health but do not cause overt neurotoxicity. Importantly, we have shown that oxysterol-activated astrocytes induce synaptotoxicity that is mediated by Lcn2. This study thus reveals new aspects of brain oxysterol effects on astrocytes and neurons, confirming their potential ability to contribute to AD pathogenesis, and providing support for further investigations into a potential role for Lcn2 as a novel therapeutic target in AD.

ABBREVIATIONS

α-EPOX: 5α,6α-epoxycholesterol; β-EPOX: 5β,6β-epoxycholesterol; 24-OHC: 24-hydroxycholesterol; 27-OHC: 27-hydroxycholesterol; 7-KC: 7-ketocholesterol; 7α-OHC: 7α-hydroxycholesterol; 7β-OHC: 7β-hydroxycholesterol; Aβ: Amyloid-β; ACM: Astrocyte conditioned media; AD: Alzheimer's disease; ApoE: Apolipoprotein E; BBB: Blood-brain barrier; CCL: C-C motif chemokine; CXCL: C-X-C motif chemokine; CYP46A1: Cholesterol 24-hydroxylase; DIV: Days *in vitro*; GC-MS: Gas chromatography-mass spectrometry; G-CSF: Granulocyte colony-stimulating factor; GFAP: Glial fibrillary acidic protein; Iba1: Ionized calcium binding adaptor molecule 1; IL: Interleukin; Lcn2: Lipocalin-2; LDH: Lactate dehydrogenase, LPS: Lipopolysaccharide; NFTs: Neurofibrillary tangles; NGAL: Neutrophil gelatinase-associated lipocalin; NMDAR: N-methyl-D-aspartate receptor; PSD: Postsynaptic density; PSD95: Postsynaptic

density protein 95; SerpinA3N: Serine protease inhibitor A3N; sICAM-1: Soluble intercellular adhesion molecule-1; siRNA: Small interfering RNA; TNF-α: Tumor necrosis factor-α.

DECLARATIONS

Ethics approval and consent to participate

All animal procedures were in accordance with the European Communities Council Directive (86/609/EEC and 2010/63/EU), the UK Animals (Scientific Procedures) Act 1986, and the Italian Law for Care and Use of Experimental Animals (26/2016), with agreement from both the King's College London (Denmark Hill) Animal Welfare and Ethical Review Board and the Ethical Committee of the University of Turin.

Consent for publication

Not applicable

Availability of data and materials

All data generated or analysed during this study are included in this published article [and its supplementary information files].

Competing interests

The authors declare that they have no competing interests.

Funding

This project was supported by funding from Alzheimer's Research UK (ARUK-RF2014-2, ARUK-EG2013-B1, ARUK-PG2019A-004), the University of Turin (RILO 2019), and Compagnia di San Paolo Foundation (CST0167048). ES was supported by Adriano Buzzati-Traverso Foundation.

Author's contributions

ES, VC and BGPN designed and performed experiments. ES and BGPN analysed samples and performed the statistical analysis. VL and CC performed GC-MS analysis and analysed data. ES and BGPN wrote the manuscript. AB, WN, and GL revised the manuscript. PG, WN, BGPN, and GL obtained the funding. ES, BGPN, GT and SG prepared the figures. All authors read and approved the final manuscript.

Acknowledgements

Not applicable

REFERENCES

1. Prince MJ WA, Guerchet MM, Ali GC, Wu YT, Prina AM, Alzheimer's Disease International. World Alzheimer Report 2015: The Global Impact of Dementia: An Analysis of Prevalence, Incidence, Cost and Trends. Alzheimer's Disease International; 2015.
2. Lane CA, Hardy J, Schott JM. Alzheimer's disease. Eur J Neurol. 2018;25:59-70.
3. Serrano-Pozo A, Frosch MP, Masliah E, Hyman BT. Neuropathological alterations in Alzheimer disease. Cold Spring Harb Perspect Med. 2011;1:a006189.

603 4. Perez-Nievas BG, Serrano-Pozo A. Deciphering the Astrocyte Reaction in Alzheimer's
604 Disease. Front Aging Neurosci. 2018;10:114.
605 5. Perez-Nievas BG, Stein TD, Tai HC, Dols-Icardo O, Scotton TC, Barroeta-Espar I, et al.
606 Dissecting phenotypic traits linked to human resilience to Alzheimer's pathology. Brain.
607 2013;136:2510-26.
608 6. Vehmas AK, Kawas CH, Stewart WF, Troncoso JC. Immune reactive cells in senile plaques
609 and cognitive decline in Alzheimer's disease. Neurobiol Aging. 2003;24:321-31.
610 7. Anderson MA, Ao Y, Sofroniew MV. Heterogeneity of reactive astrocytes. Neurosci Lett.
611 2014;565:23-9.
612 8. Zamanian JL, Xu L, Foo LC, Nouri N, Zhou L, Giffard RG, et al. Genomic analysis of reactive
613 astrogliosis. J Neurosci. 2012;32:6391-410.
614 9. Iram T, Trudler D, Kain D, Kanner S, Galron R, Vassar R, et al. Astrocytes from old
615 Alzheimer's disease mice are impaired in Abeta uptake and in neuroprotection. Neurobiol Dis.
616 2016;96:84-94.
617 10. Liddelow SA, Guttenplan KA, Clarke LE, Bennett FC, Bohlen CJ, Schirmer L, et al.
618 Neurotoxic reactive astrocytes are induced by activated microglia. Nature. 2017;541:481-7.
619 11. Garwood CJ, Pooler AM, Atherton J, Hanger DP, Noble W. Astrocytes are important
620 mediators of Abeta-induced neurotoxicity and tau phosphorylation in primary culture. Cell Death Dis.
621 2011;2:e167.
622 12. Cavanagh C, Tse YC, Nguyen HB, Krantic S, Breitner JC, Quirion R, et al. Inhibiting tumor
623 necrosis factor-alpha before amyloidosis prevents synaptic deficits in an Alzheimer's disease model.
624 Neurobiol Aging. 2016;47:41-9.
625 13. Lian H, Yang L, Cole A, Sun L, Chiang AC, Fowler SW, et al. NFkappaB-activated astroglial
626 release of complement C3 compromises neuronal morphology and function associated with
627 Alzheimer's disease. Neuron. 2015;85:101-15.

628 14. Jha MK, Lee S, Park DH, Kook H, Park KG, Lee IK, et al. Diverse functional roles of
629 lipocalin-2 in the central nervous system. Neurosci Biobehav Rev. 2015;49:135-56.
630 15. Naude PJ, Nyakas C, Eiden LE, Ait-Ali D, van der Heide R, Engelborghs S, et al. Lipocalin
631 2: novel component of proinflammatory signaling in Alzheimer's disease. FASEB J. 2012;26:2811-
632 23.
633 16. Ferreira AC, Da Mesquita S, Sousa JC, Correia-Neves M, Sousa N, Palha JA, et al. From the
634 periphery to the brain: Lipocalin-2, a friend or foe? Prog Neurobiol. 2015;131:120-36.
635 17. Bi F, Huang C, Tong J, Qiu G, Huang B, Wu Q, et al. Reactive astrocytes secrete lcn2 to
636 promote neuron death. Proc Natl Acad Sci U S A. 2013;110:4069-74.
637 18. Alzheimer A, Stelzmann RA, Schnitzlein HN, Murtagh FR. An English translation of
638 Alzheimer's 1907 paper, "Uber eine eigenartige Erkankung der Hirnrinde". Clin Anat. 1995;8:429-
639 31.
640 19. Corder EH, Saunders AM, Strittmatter WJ, Schmechel DE, Gaskell PC, Small GW, et al.
641 Gene dose of apolipoprotein E type 4 allele and the risk of Alzheimer's disease in late onset families.
642 Science. 1993;261:921-3.
643 20. Di Paolo G, Kim TW. Linking lipids to Alzheimer's disease: cholesterol and beyond. Nat Rev
644 Neurosci. 2011;12:284-96.
645 21. Wood WG, Li L, Muller WE, Eckert GP. Cholesterol as a causative factor in Alzheimer's
646 disease: a debatable hypothesis. J Neurochem. 2014;129:559-72.
647 22. Gamba P, Testa G, Gargiulo S, Staurenghi E, Poli G, Leonarduzzi G. Oxidized cholesterol as
648 the driving force behind the development of Alzheimer's disease. Front Aging Neurosci. 2015;7.
649 23. Dason JS, Smith AJ, Marin L, Charlton MP. Cholesterol and F-actin are required for clustering
650 of recycling synaptic vesicle proteins in the presynaptic plasma membrane. J Physiol. 2014;592:621-
651 33.

652 24. van Deijk AF, Camargo N, Timmerman J, Heistek T, Brouwers JF, Mogavero F, et al.
653 Astrocyte lipid metabolism is critical for synapse development and function in vivo. Glia.
654 2017;65:670-82.
655 25. Lutjohann D, Breuer O, Ahlborg G, Nennesmo I, Siden A, Diczfalusy U, et al. Cholesterol
656 homeostasis in human brain: evidence for an age-dependent flux of 24S-hydroxycholesterol from the
657 brain into the circulation. Proc Natl Acad Sci U S A. 1996;93:9799-804.
658 26. Iuliano L, Crick PJ, Zerbinati C, Tritapepe L, Abdel-Khalik J, Poirot M, et al. Cholesterol
659 metabolites exported from human brain. Steroids. 2015;99:189-93.
660 27. Testa G, Staurenghi E, Zerbinati C, Gargiulo S, Iuliano L, Giaccone G, et al. Changes in brain
661 oxysterols at different stages of Alzheimer's disease: Their involvement in neuroinflammation. Redox
662 Biol. 2016;10:24-33.
663 28. Mutemberezi V, Guillemot-Legris O, Muccioli GG. Oxysterols: From cholesterol metabolites
664 to key mediators. Prog Lipid Res. 2016;64:152-69.
665 29. Testa G, Gamba P, Badilli U, Gargiulo S, Maina M, Guina T, et al. Loading into nanoparticles
666 improves quercetin's efficacy in preventing neuroinflammation induced by oxysterols. PLoS One.
667 2014;9:e96795.
668 30. Zhang X, Xi Y, Yu H, An Y, Wang Y, Tao L, et al. 27-hydroxycholesterol promotes Abeta
669 accumulation via altering Abeta metabolism in mild cognitive impairment patients and APP/PS1
670 mice. Brain Pathol. 2019;29:558-73.
671 31. Gamba P, Leonarduzzi G, Tamagno E, Guglielmotto M, Testa G, Sottero B, et al. Interaction
672 between 24-hydroxycholesterol, oxidative stress, and amyloid-beta in amplifying neuronal damage
673 in Alzheimer's disease: three partners in crime. Aging Cell. 2011;10:403-17.
674 32. Marwarha G, Dasari B, Prasanthi JR, Schommer J, Ghribi O. Leptin reduces the accumulation
675 of Abeta and phosphorylated tau induced by 27-hydroxycholesterol in rabbit organotypic slices. J
676 Alzheimers Dis. 2010;19:1007-19.

677 33. Merino-Serrais P, Loera-Valencia R, Rodriguez-Rodriguez P, Parrado-Fernandez C, Ismail
678 MA, Maioli S, et al. 27-Hydroxycholesterol Induces Aberrant Morphology and Synaptic Dysfunction
679 in Hippocampal Neurons. Cereb Cortex. 2019;29:429-46.
680 34. Jang ER, Lee CS. 7-ketocholesterol induces apoptosis in differentiated PC12 cells via reactive
681 oxygen species-dependent activation of NF-kappaB and Akt pathways. Neurochem Int. 2011;58:52-
682 9.
683 35. Nury T, Samadi M, Zarrouk A, Riedinger JM, Lizard G. Improved synthesis and in vitro
684 evaluation of the cytotoxic profile of oxysterols oxidized at C4 (4alpha- and 4beta-
685 hydroxycholesterol) and C7 (7-ketocholesterol, 7alpha- and 7beta-hydroxycholesterol) on cells of the
686 central nervous system. Eur J Med Chem. 2013;70:558-67.
687 36. An Y, Zhang DD, Yu HL, Ma WW, Lu YH, Liu QR, et al. 27-Hydroxycholesterol regulates
688 cholesterol synthesis and transport in C6 glioma cells. Neurotoxicology. 2017;59:88-97.
689 37. Abildayeva K, Jansen PJ, Hirsch-Reinshagen V, Bloks VW, Bakker AH, Ramaekers FC, et
690 al. 24(S)-hydroxycholesterol participates in a liver X receptor-controlled pathway in astrocytes that
691 regulates apolipoprotein E-mediated cholesterol efflux. J Biol Chem. 2006;281:12799-808.
692 38. Zhang DD, Yu HL, Ma WW, Liu QR, Han J, Wang H, et al. 27-Hydroxycholesterol
693 contributes to disruptive effects on learning and memory by modulating cholesterol metabolism in
694 the rat brain. Neuroscience. 2015;300:163-73.
695 39. Ma WW, Li CQ, Yu HL, Zhang DD, Xi YD, Han J, et al. The oxysterol 27-hydroxycholesterol
696 increases oxidative stress and regulate Nrf2 signaling pathway in astrocyte cells. Neurochem Res.
697 2015;40:758-66.
698 40. Cigliano L, Spagnuolo MS, Napolitano G, Iannotta L, Fasciolo G, Barone D, et al. 24S-
699 hydroxycholesterol affects redox homeostasis in human glial U-87MG cells. Mol Cell Endocrinol.
700 2019;486:25-33.

41. Bochelen D, Langley K, Adamczyk M, Kupferberg A, Hor F, Vincendon G, et al. 7beta-hydroxysterol is cytotoxic to neonatal rat astrocytes in primary culture when cAMP levels are increased. J Neurosci Res. 2000;62:99-111.

42. Schildge S, Bohrer C, Beck K, Schachtrup C. Isolation and culture of mouse cortical astrocytes. J Vis Exp. 2013.

43. Hudry E, Wu HY, Arbel-Ornath M, Hashimoto T, Matsouaka R, Fan Z, et al. Inhibition of the NFAT pathway alleviates amyloid beta neurotoxicity in a mouse model of Alzheimer's disease. J Neurosci. 2012;32:3176-92.

44. Leoni V, Strittmatter L, Zorzi G, Zibordi F, Dusi S, Garavaglia B, et al. Metabolic consequences of mitochondrial coenzyme A deficiency in patients with PANK2 mutations. Mol Genet Metab. 2012;105:463-71.

45. Livak KJ, Schmittgen TD. Analysis of relative gene expression data using real-time quantitative PCR and the 2(-Delta Delta C(T)) Method. Methods. 2001;25:402-8.

46. Sovrea AS, Bosca AB. Astrocytes reassessment - an evolving concept part one: embryology, biology, morphology and reactivity. J Mol Psychiatry. 2013;1:18.

47. Liddelow SA, Barres BA. Reactive Astrocytes: Production, Function, and Therapeutic Potential. Immunity. 2017;46:957-67.

48. Sofroniew MV. Multiple roles for astrocytes as effectors of cytokines and inflammatory mediators. Neuroscientist. 2014;20:160-72.

49. Kim JH, Ko PW, Lee HW, Jeong JY, Lee MG, Kim JH, et al. Astrocyte-derived lipocalin-2 mediates hippocampal damage and cognitive deficits in experimental models of vascular dementia. Glia. 2017;65:1471-90.

50. Lordan S, Mackrill JJ, O'Brien NM. Oxysterols and mechanisms of apoptotic signaling: implications in the pathology of degenerative diseases. J Nutr Biochem. 2009;20:321-36.

51. D'Amelio M, Sheng M, Cecconi F. Caspase-3 in the central nervous system: beyond apoptosis. Trends Neurosci. 2012;35:700-9.

52. Mucha M, Skrzypiec AE, Schiavon E, Attwood BK, Kucerova E, Pawlak R. Lipocalin-2 controls neuronal excitability and anxiety by regulating dendritic spine formation and maturation. Proc Natl Acad Sci U S A. 2011;108:18436-41.

53. Lee S, Lee WH, Lee MS, Mori K, Suk K. Regulation by lipocalin-2 of neuronal cell death, migration, and morphology. J Neurosci Res. 2012;90:540-50.

54. Karch CM, Goate AM. Alzheimer's disease risk genes and mechanisms of disease pathogenesis. Biol Psychiatry. 2015;77:43-51.

55. Serrano-Pozo A, Mielke ML, Gomez-Isla T, Betensky RA, Growdon JH, Frosch MP, et al. Reactive glia not only associates with plaques but also parallels tangles in Alzheimer's disease. Am J Pathol. 2011;179:1373-84.

56. Boisvert MM, Erikson GA, Shokhirev MN, Allen NJ. The Aging Astrocyte Transcriptome from Multiple Regions of the Mouse Brain. Cell Rep. 2018;22:269-85.

57. Lee S, Park JY, Lee WH, Kim H, Park HC, Mori K, et al. Lipocalin-2 is an autocrine mediator of reactive astrocytosis. J Neurosci. 2009;29:234-49.

58. Holtje M, Hoffmann A, Hofmann F, Mucke C, Grosse G, Van Rooijen N, et al. Role of Rho GTPase in astrocyte morphology and migratory response during in vitro wound healing. J Neurochem. 2005;95:1237-48.

59. Styren SD, Kamboh MI, DeKosky ST. Expression of differential immune factors in temporal cortex and cerebellum: the role of alpha-1-antichymotrypsin, apolipoprotein E, and reactive glia in the progression of Alzheimer's disease. J Comp Neurol. 1998;396:511-20.

60. Padmanabhan J, Levy M, Dickson DW, Potter H. Alpha1-antichymotrypsin, an inflammatory protein overexpressed in Alzheimer's disease brain, induces tau phosphorylation in neurons. Brain. 2006;129:3020-34.

61. Rutkowska A, Shimshek DR, Sailer AW, Dev KK. EBI2 regulates pro-inflammatory signalling and cytokine release in astrocytes. Neuropharmacology. 2018;133:121-8.

752 62. Mutemberezi V, Buisseret B, Masquelier J, Guillemot-Legris O, Alhouayek M, Muccioli GG.
753 Oxysterol levels and metabolism in the course of neuroinflammation: insights from in vitro and in
754 vivo models. J Neuroinflammation. 2018;15:74.
755 63. van Gijsel-Bonnello M, Baranger K, Benech P, Rivera S, Khrestchatisky M, de Reggi M, et
756 al. Metabolic changes and inflammation in cultured astrocytes from the 5xFAD mouse model of
757 Alzheimer's disease: Alleviation by pantethine. PLoS One. 2017;12:e0175369.
758 64. Choi SS, Lee HJ, Lim I, Satoh J, Kim SU. Human astrocytes: secretome profiles of cytokines
759 and chemokines. PLoS One. 2014;9:e92325.
760 65. Sharma V, Mishra M, Ghosh S, Tewari R, Basu A, Seth P, et al. Modulation of interleukin-
761 1beta mediated inflammatory response in human astrocytes by flavonoids: implications in
762 neuroprotection. Brain Res Bull. 2007;73:55-63.
763 66. Morales I, Guzman-Martinez L, Cerda-Troncoso C, Farias GA, Maccioni RB.
764 Neuroinflammation in the pathogenesis of Alzheimer's disease. A rational framework for the search
765 of novel therapeutic approaches. Front Cell Neurosci. 2014;8:112.
766 67. Hubbard AK, Rothlein R. Intercellular adhesion molecule-1 (ICAM-1) expression and cell
767 signaling cascades. Free Radic Biol Med. 2000;28:1379-86.
768 68. Lyons PD, Benveniste EN. Cleavage of membrane-associated ICAM-1 from astrocytes:
769 involvement of a metalloprotease. Glia. 1998;22:103-12.
770 69. Otto VI, Gloor SM, Frentzel S, Gilli U, Ammann E, Hein AE, et al. The production of
771 macrophage inflammatory protein-2 induced by soluble intercellular adhesion molecule-1 in mouse
772 astrocytes is mediated by src tyrosine kinases and p42/44 mitogen-activated protein kinase. J
773 Neurochem. 2002;80:824-34.
774 70. Lawson C, Wolf S. ICAM-1 signaling in endothelial cells. Pharmacol Rep. 2009;61(1):22-32.
775 71. Trombetta BA, Carlyle BC, Koenig AM, Shaw LM, Trojanowski JQ, Wolk DA, et al. The
776 technical reliability and biotemporal stability of cerebrospinal fluid biomarkers for profiling multiple
777 pathophysiologies in Alzheimer's disease. PLoS One. 2018;13:e0193707.

778 72. Janelidze S, Mattsson N, Stomrud E, Lindberg O, Palmqvist S, Zetterberg H, et al. CSF
779 biomarkers of neuroinflammation and cerebrovascular dysfunction in early Alzheimer disease.
780 Neurology. 2018;91:e867-e77.
781 73. Allaman I, Gavillet M, Belanger M, Laroche T, Viertl D, Lashuel HA, et al. Amyloid-beta
782 aggregates cause alterations of astrocytic metabolic phenotype: impact on neuronal viability. J
783 Neurosci. 2010;30:3326-38.
784 74. Sheng M. The postsynaptic NMDA-receptor--PSD-95 signaling complex in excitatory
785 synapses of the brain. J Cell Sci. 2001;114:1251.
786 75. Prieto GA, Cotman CW. Cytokines and cytokine networks target neurons to modulate long-
787 term potentiation. Cytokine Growth Factor Rev. 2017;34:27-33.
788 76. Khairova RA, Machado-Vieira R, Du J, Manji HK. A potential role for pro-inflammatory
789 cytokines in regulating synaptic plasticity in major depressive disorder. Int J Neuropsychopharmacol.
790 2009;12:561-78.
791 77. Turner MD, Nedjai B, Hurst T, Pennington DJ. Cytokines and chemokines: At the crossroads
792 of cell signalling and inflammatory disease. Biochim Biophys Acta. 2014;1843(11):2563-82.
793 78. Mao LM, Wang JQ. Synaptically Localized Mitogen-Activated Protein Kinases: Local
794 Substrates and Regulation. Mol Neurobiol. 2016;53:6309-15.
795 79. Paul SM, Doherty JJ, Robichaud AJ, Belfort GM, Chow BY, Hammond RS, et al. The major
796 brain cholesterol metabolite 24(S)-hydroxycholesterol is a potent allosteric modulator of N-methyl-
797 D-aspartate receptors. J Neurosci. 2013;33:17290-300.
798 80. Kulig W, Cwiklik L, Jurkiewicz P, Rog T, Vattulainen I. Cholesterol oxidation products and
799 their biological importance. Chem Phys Lipids. 2016;199:144-60.
800 81. Dias IH, Borah K, Amin B, Griffiths HR, Sassi K, Lizard G, et al. Localisation of oxysterols
801 at the sub-cellular level and in biological fluids. J Steroid Biochem Mol Biol. 2019;193:105426.
802 82. Perez MJ, Vergara-Pulgar K, Jara C, Cabezas-Opazo F, Quintanilla RA. Caspase-Cleaved Tau
803 Impairs Mitochondrial Dynamics in Alzheimer's Disease. Mol Neurobiol. 2018;55:1004-18.

804 83. D'Amelio M, Cavallucci V, Middei S, Marchetti C, Pacioni S, Ferri A, et al. Caspase-3 triggers
805 early synaptic dysfunction in a mouse model of Alzheimer's disease. Nat Neurosci. 2011;14:69-76.
806 84. Noble W, Garwood C, Stephenson J, Kinsey AM, Hanger DP, Anderton BH. Minocycline
807 reduces the development of abnormal tau species in models of Alzheimer's disease. FASEB J.
808 2009;23:739-50.
809 85. Ragot K, Delmas D, Athias A, Nury T, Baarine M, Lizard G. alpha-Tocopherol impairs 7-
810 ketocholesterol-induced caspase-3-dependent apoptosis involving GSK-3 activation and Mcl-1
811 degradation on 158N murine oligodendrocytes. Chem Phys Lipids. 2011;164:469-78.
812 86. Nakazawa T, Miyanoki Y, Urano Y, Uehara M, Saito Y, Noguchi N. Effect of vitamin E on
813 24(S)-hydroxycholesterol-induced necroptosis-like cell death and apoptosis. J Steroid Biochem Mol
814 Biol. 2017;169:69-76.
815 87. Kim A, Nam YJ, Lee CS. Taxifolin reduces the cholesterol oxidation product-induced
816 neuronal apoptosis by suppressing the Akt and NF-kappaB activation-mediated cell death. Brain Res
817 Bull. 2017;134:63-71.
818 88. DeKosky ST, Scheff SW. Synapse loss in frontal cortex biopsies in Alzheimer's disease:
819 correlation with cognitive severity. Ann Neurol. 1990;27:457-64.
820 89. Crimins JL, Pooler A, Polydoro M, Luebke JI, Spires-Jones TL. The intersection of amyloid
821 beta and tau in glutamatergic synaptic dysfunction and collapse in Alzheimer's disease. Ageing Res
822 Rev. 2013;12:757-63.
823

824 **FIGURE LEGENDS**

825 **Fig. 1 Dose-response experiments to test the effect of the oxysterol mixtures on astrocyte**
826 **viability and morphology.** Primary astrocyte cultures were treated with the Early or Late AD
827 oxysterol mixture (1, 5, or 10 μM), or vehicle (ethanol) for 24h. **(A)** The bar graph shows the lactate
828 dehydrogenase (LDH) release from treated astrocytes. Values are the proportion of LDH released

829 into medium relative to total LDH in lysed cells normalized to values for control media. Data are
830 expressed as mean ± SD from three different experiments (n=9, one-way ANOVA). **(B)** Astrocyte
831 morphology was examined by immunocytochemistry using a glial fibrillary acidic protein (GFAP)
832 antibody (red) and nuclei were stained with Hoechst 33258 (blue). Representative images from three
833 experiments are shown. Cells were imaged using an LSM800 confocal microscope (Zeiss; 40X
834 objective; scale bar: 100 μm).

835

836 **Fig. 2 Oxysterol mixtures induce a clear morphological change in astrocytes.** Primary astrocytes
837 were treated with 10 μM of the Early or Late AD oxysterol mixture for up to 24h. Astrocyte
838 morphology was examined by immunocytochemistry using a glial fibrillary acidic protein (GFAP)
839 antibody (red) and nuclei were stained with Hoechst 33258 (blue). Representative images from three
840 experiments are shown. Cells were imaged using an Eclipse Ti-E Microscope (Nikon; 20X objective;
841 scale bar: 100 μm).

842

843 **Fig. 3 Oxysterol mixtures increase the synthesis of pan-reactive astrocyte markers.** The glial
844 fibrillary acidic protein (GFAP), serine protease inhibitor A3N (SerpinA3N), and lipocalin-2 (Lcn2)
845 protein levels were determined by Western blotting of lysates from primary astrocytes treated with
846 10 μM of the Early or Late AD oxysterol mixture for up to 24h. The amounts of proteins of interest
847 were normalized to β-actin levels in the same sample and are represented as percentage of average
848 control values. Data are expressed as mean values ± SD of three different experiments (n=9, one-way
849 ANOVA). ****P<0.0001, ***P<0.001, *P<0.05 vs. control.

850

851 **Fig. 4 Oxysterol treatment increases the release of lipocalin-2 (Lcn2), cytokines and chemokines**
852 **from astrocytes.** Astrocyte cultures were treated with the Early or Late AD oxysterol mixture (10

μM) for 24h. **(A)** Lcn2 protein levels in astrocyte conditioned media (ACM) were examined by Western blotting. Data are expressed as mean values ± SD from three different experiments and are shown as percentage change from average control values (n=9, one-way ANOVA). ****P<0.0001 vs control. **(B)** Mouse cytokine profiler antibody arrays were used to detect the amounts of 40 mediators in ACM. Representative images of array membranes are shown, highlighted some of the cytokines found to be significantly increased in ACM from treated cells. The bar chart shows the cytokines significantly affected by oxysterol mixture treatments as percentage change from control. Data are expressed as mean values ± SD from three different experiments (n=6, one-way ANOVA). ***P<0.001, **P<0.01, and *P<0.05 vs control.

Fig. 5 Oxysterol-stimulated astrocytes compromise neuronal health. Primary neurons (13 DIV) were treated with the Late AD oxysterol mixture (10 μM) for 24h or they were co-cultured for 24h with astrocytes grown on cell culture inserts that had been previously treated with the same oxysterol mixture for 12h. **(A)** Graphical representation of co-culture experiments. **(B)** The protein levels of the postsynaptic density protein 95 (PSD95), synapsin, and cleaved caspase-3 were determined by Western blotting. Data were normalized to the corresponding β-actin levels. Data are expressed as mean values ± SD of three different experiments as percentage change from respective control (n=9, Student's t-test). **P<0.01 and *P<0.05 vs control.

Fig. 6 Lipocalin-2 (Lcn2) gene silencing prevents Lcn2 upregulation and release into the medium. Astrocyte cultures were transfected for 6h with Lcn2 or scrambled siRNA and then treated with the Late AD oxysterol mixture 10 μM (Mix) for 12h. After treatment, the medium was changed and astrocytes were incubated with fresh medium for 24h. Transient Lcn2 gene knockdown was evaluated by **(A)** real-time RT-PCR and **(B)** Western blotting of both lysates and astrocyte

conditioned media (ACM) samples. Data were normalized to the corresponding β-actin levels. Data are expressed as mean values ± SD from three different experiments as percentage change from control (n=9, one-way ANOVA). ****P<0.0001, ***P<0.001, and *P<0.05 vs control; #### P<0.0001 vs oxysterol treated. **(C)** Astrocyte morphology was examined by immunocytochemistry using a glial fibrillary acidic protein (GFAP) antibody (red) and nuclei were stained with Hoechst 33258 (blue). Representative images from three experiments are shown. Cells were imaged using an LSM800 confocal microscope (Zeiss, 40X objective; scale bar: 100 μm).

Fig. 7 Lipocalin-2 (Lcn2) secreted by oxysterol-stimulated astrocytes affects neurite complexity and decreases dendritic spine density. Primary neurons were incubated for 24h with conditioned media from astrocytes transfected for 6h with Lcn2 or scrambled siRNA and then treated with the Late AD oxysterol mixture 10 μM for 12h. After treatment, the medium was changed and astrocytes were incubated with fresh medium for 24h. High resolution digital images of live neurons were obtained using an Opera-Phenix microscope (Perkin-Elmer). **(A)** Neurite complexity was analysed using Harmony software. Total and maximum neurite length, number of nodes and extremities were quantified and compared between groups. Representative images are shown (scale bar: 100 μm). Data are expressed as mean values ± SD from three different experiments and were obtained from analysis of 20 neurons/condition (one-way ANOVA). *P<0.05 vs control. **(B)** NeuronStudio software was used for dendritic spine analysis. Spine density was defined as number of spines per micrometer of dendrite length and was obtained from analysis of 20 neurons/condition (one-way ANOVA). Representative images are shown (scale bar: 25 μm). Data are expressed as mean values ± SD from three different experiments. ***P<0.001 vs control.

ADDITIONAL FILES

Additional file 1

TIFF

Supplemental Fig. 1 Evaluation of astrocyte culture purity. Astrocytic cultures were analysed by **(A)** immunocytochemistry and **(B)** Western blotting using antibodies against glial fibrillary acidic protein (GFAP, astrocytic marker) and ionized calcium binding adaptor molecule 1 (Iba1, microglial marker). Cells were imaged using an LSM800 confocal microscope (Zeiss, 40X objective; scale bar: 100 μm).

Additional file 2

TIFF

Supplemental Fig. 2 Validation of lipocalin-2 (Lcn2) silencing efficiency. Astrocyte cultures were transfected for 6h with Lcn2 or scrambled siRNA, then the medium was changed and astrocytes were incubated with fresh medium for 36h. Transient Lcn2 gene knockdown was evaluated by real-time RT-PCR. Data were normalized to the corresponding β-actin levels. Data are expressed as mean values ± SD of three different experiments (n=9, one-way ANOVA). ****P<0.0001 vs control.

Additional file 3

TIFF

Supplemental Fig. 3 Oxysterol analyses in astrocyte culture media. Astrocyte cultures were treated for 1, 3, 12 or 24h with the Early or Late AD oxysterol mixtures (10 μM). Astrocyte conditioned media was collected and the amounts of the seven oxysterols present in the mixtures were determined by gas chromatography-mass spectrometry (GC-MS). The graph shows the amounts of oxysterol in media expressed as percentage of the original oxysterol concentrations present in each

924 mixture. Data shown are averages of the measurements obtained from treatments with Early and Late
925 AD mixtures. Data are expressed as mean values ± SD from two different experiments (n=6).

926

927 **Additional file 4**

928 TIFF

929 **Supplemental Fig. 4 Oxysterol mixtures do not directly cause neuron death.** Neuronal viability
930 was assessed in neurons treated with the Early or Late AD oxysterol mixture (10 μM) for 24h. The
931 bar graph shows the proportion of lactate dehydrogenase (LDH) released into medium relative to total
932 LDH in lysed cells, normalized to values for control media. Data are expressed as mean values ± SD
933 from three different experiments (n=12, one-way ANOVA).

934

935

936

937

Figures

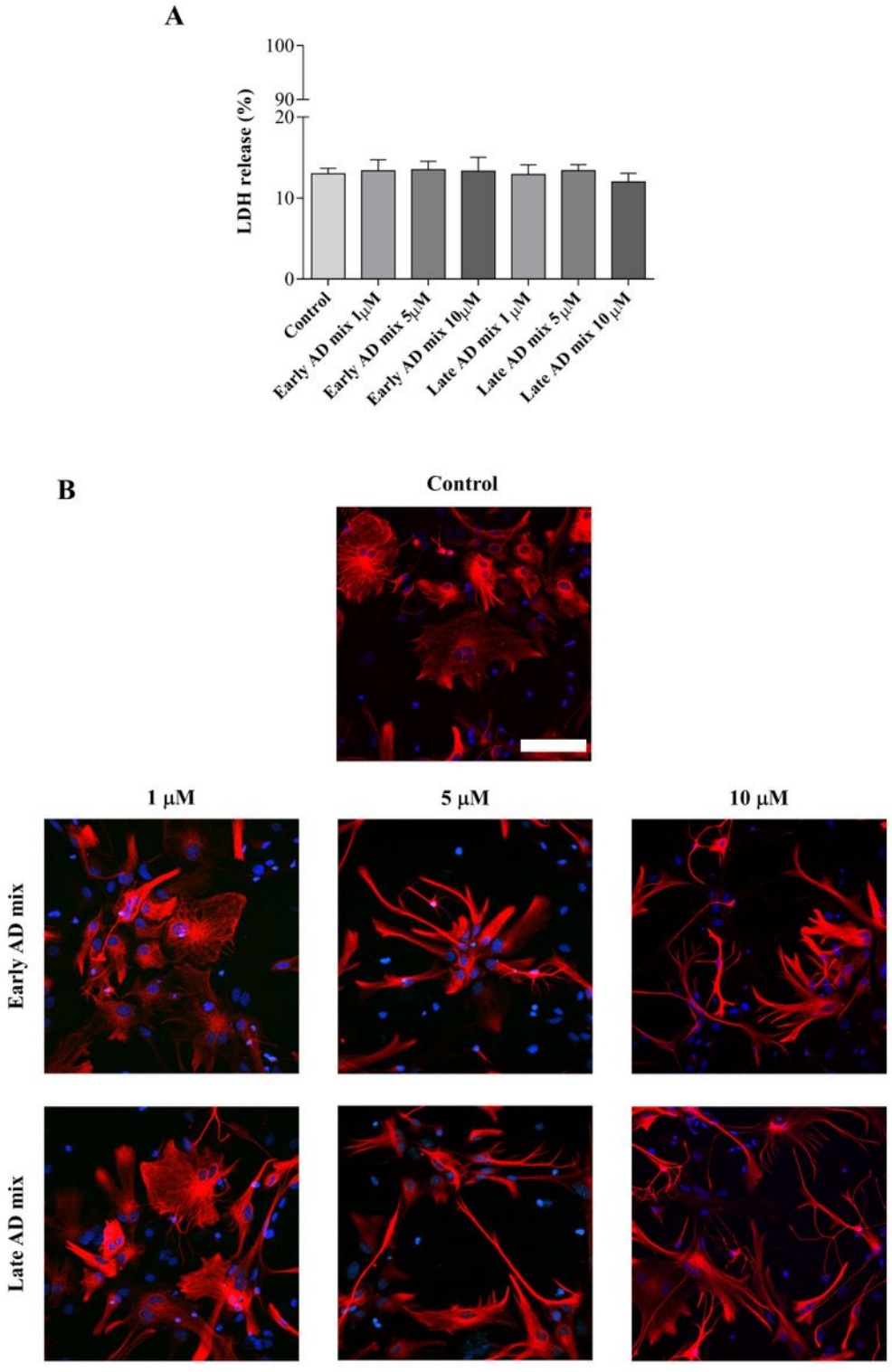

Figure 1

Dose-response experiments to test the effect of the oxysterol mixtures on astrocyte viability and morphology. Primary astrocyte cultures were treated with the Early or Late AD oxysterol mixture (1, 5, or 10 μM), or vehicle (ethanol) for 24h. (A) The bar graph shows the lactate dehydrogenase (LDH) release

from treated astrocytes. Values are the proportion of LDH released into medium relative to total LDH in lysed cells normalized to values for control media. Data are expressed as mean ± SD from three different experiments (n=9, one-way ANOVA). (B) Astrocyte morphology was examined by immunocytochemistry using a glial fibrillary acidic protein (GFAP) antibody (red) and nuclei were stained with Hoechst 33258 (blue). Representative images from three experiments are shown. Cells were imaged using an LSM800 confocal microscope (Zeiss; 40X objective; scale bar: 100 □m).

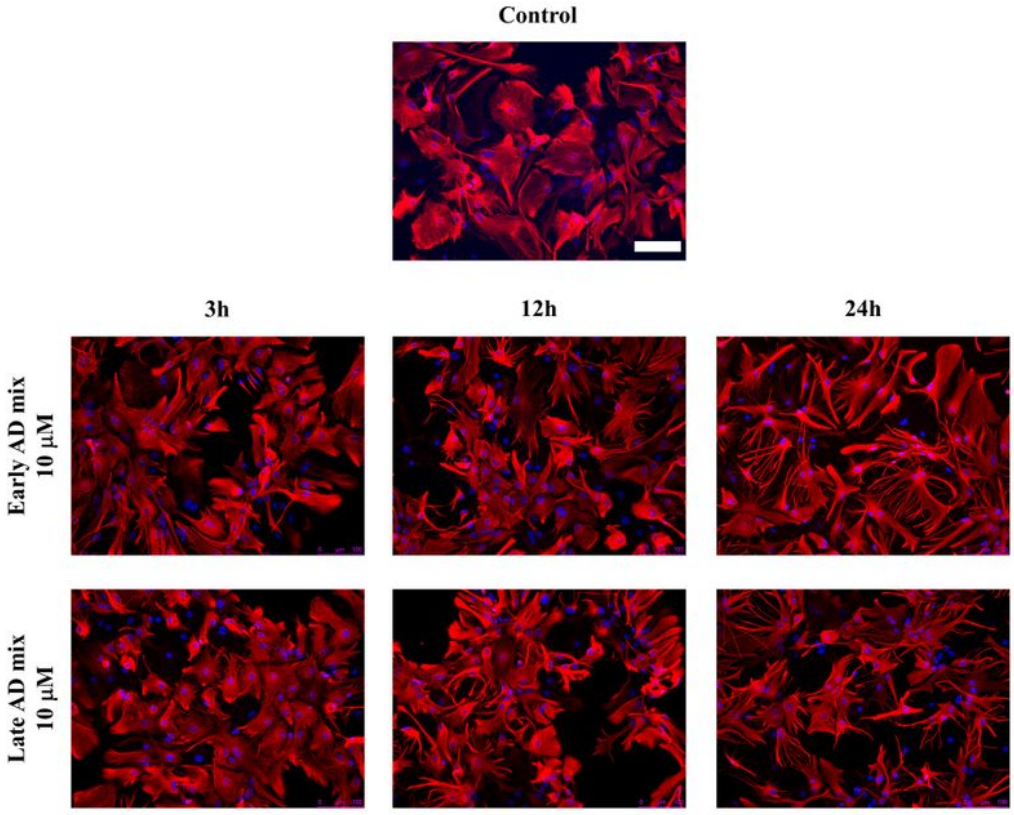

Figure 2

Oxysterol mixtures induce a clear morphological change in astrocytes. Primary astrocytes were treated with 10 □M of the Early or Late AD oxysterol mixture for up to 24h. Astrocyte morphology was examined by immunocytochemistry using a glial fibrillary acidic protein (GFAP) antibody (red) and nuclei were stained with Hoechst 33258 (blue). Representative images from three experiments are shown. Cells were imaged using an Eclipse Ti-E Microscope (Nikon; 20X objective; scale bar: 100 □m).

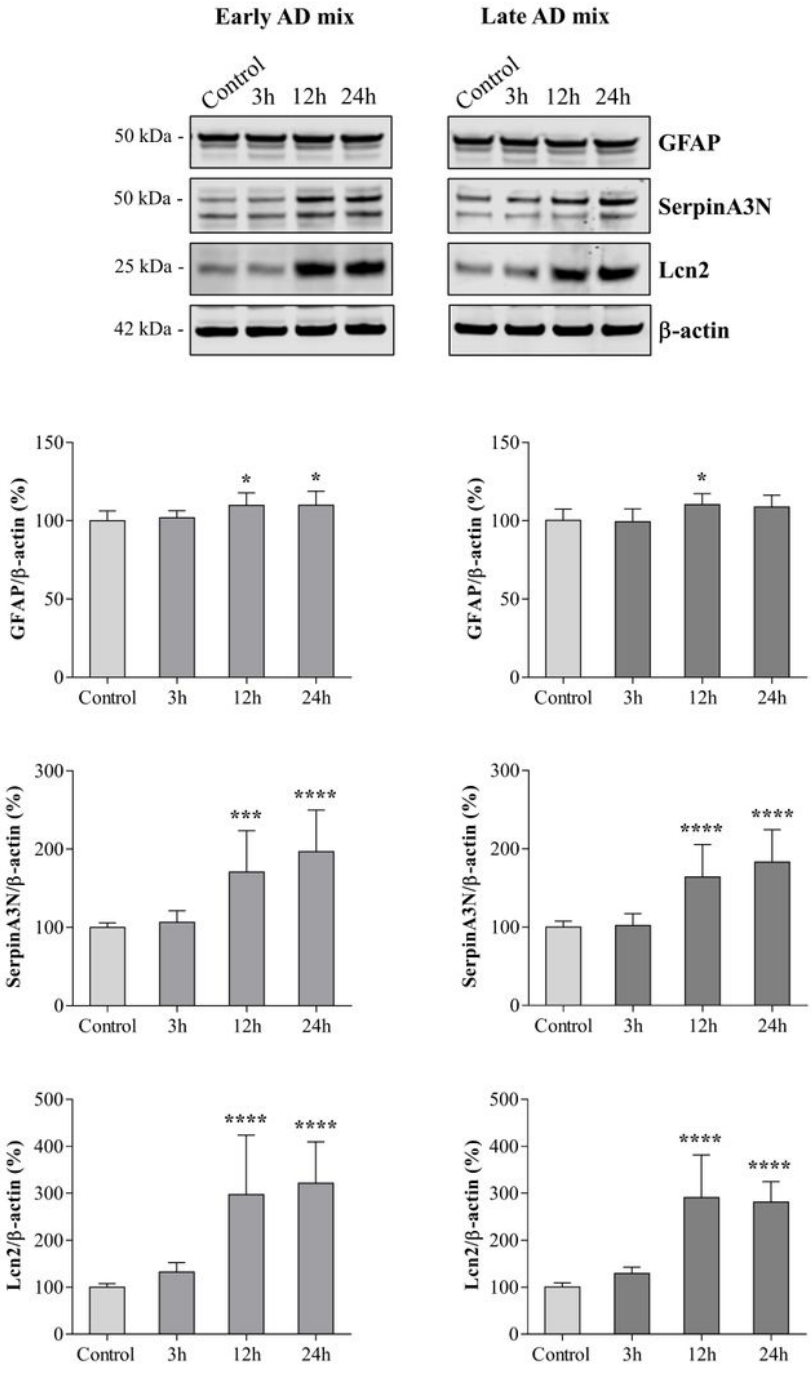

Figure 3

Oxysterol mixtures increase the synthesis of pan-reactive astrocyte markers. The glial fibrillary acidic protein (GFAP), serine protease inhibitor A3N (SerpinA3N), and lipocalin-2 (Lcn2) protein levels were determined by Western blotting of lysates from primary astrocytes treated with 10 □M of the Early or Late AD oxysterol mixture for up to 24h. The amounts of proteins of interest were normalized to □-actin levels in the same sample and are represented as percentage of average control values. Data are expressed as mean values ± SD of three different experiments (n=9, one-way ANOVA). ****P<0.0001, ***P<0.001, *P<0.05 vs. control.

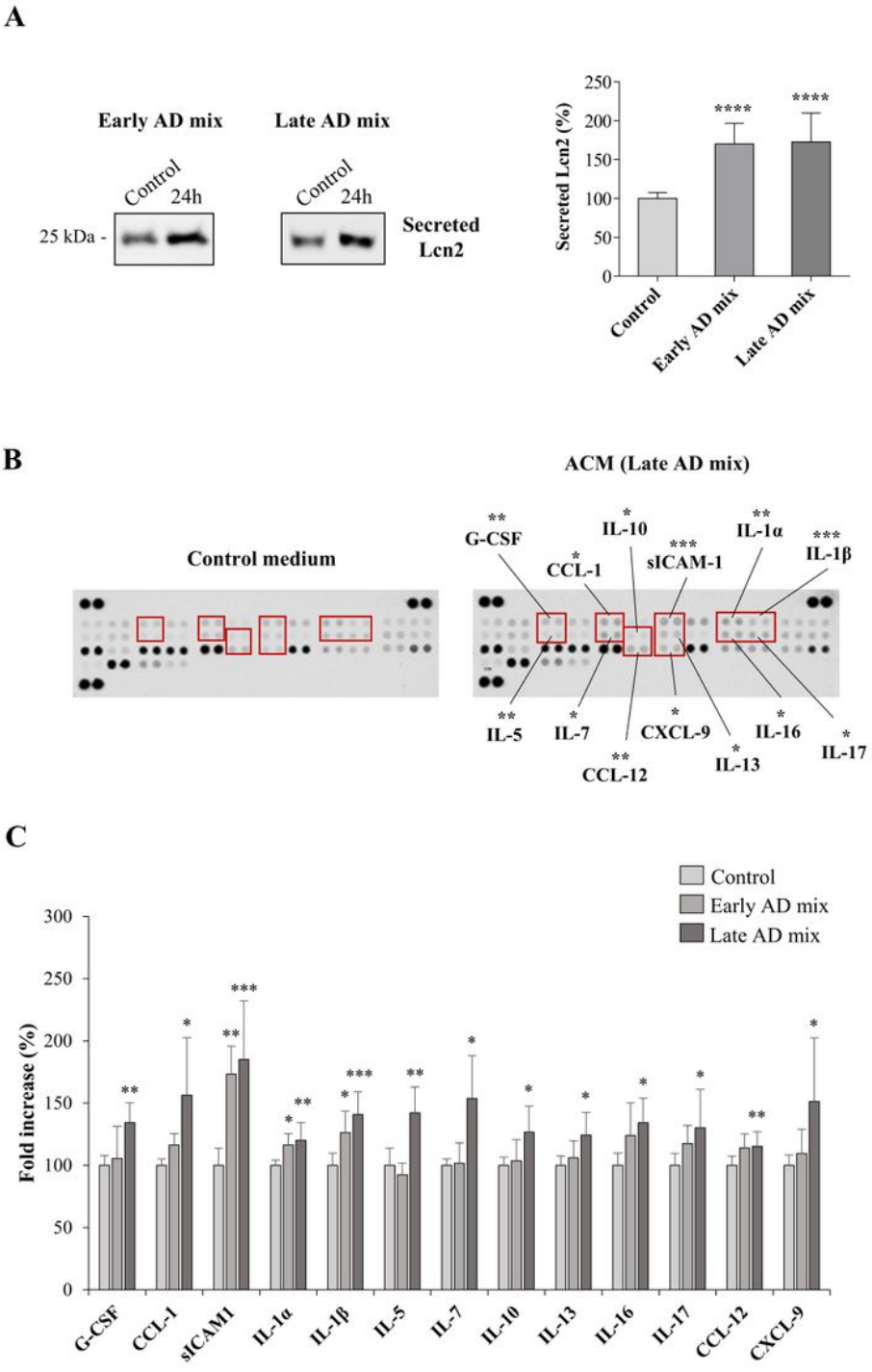

Figure 4

Oxysterol treatment increases the release of lipocalin-2 (Lcn2), cytokines and chemokines from astrocytes. Astrocyte cultures were treated with the Early or Late AD oxysterol mixture (10 □M) for 24h. (A) Lcn2 protein levels in astrocyte conditioned media (ACM) were examined by Western blotting. Data are expressed as mean values ± SD from three different experiments and are shown as percentage change from average control values (n=9, one-way ANOVA). ****P<0.0001 vs control. (B) Mouse cytokine profiler antibody arrays were used to detect the amounts of 40 mediators in ACM. Representative images of array membranes are shown, highlighted some of the cytokines found to be significantly increased in ACM from treated cells. The bar chart shows the cytokines significantly affected by oxysterol mixture treatments as percentage change from control. Data are expressed as mean values ± SD from three different experiments (n=6, one-way ANOVA). ***P<0.001, **P<0.01, and *P<0.05 vs control.

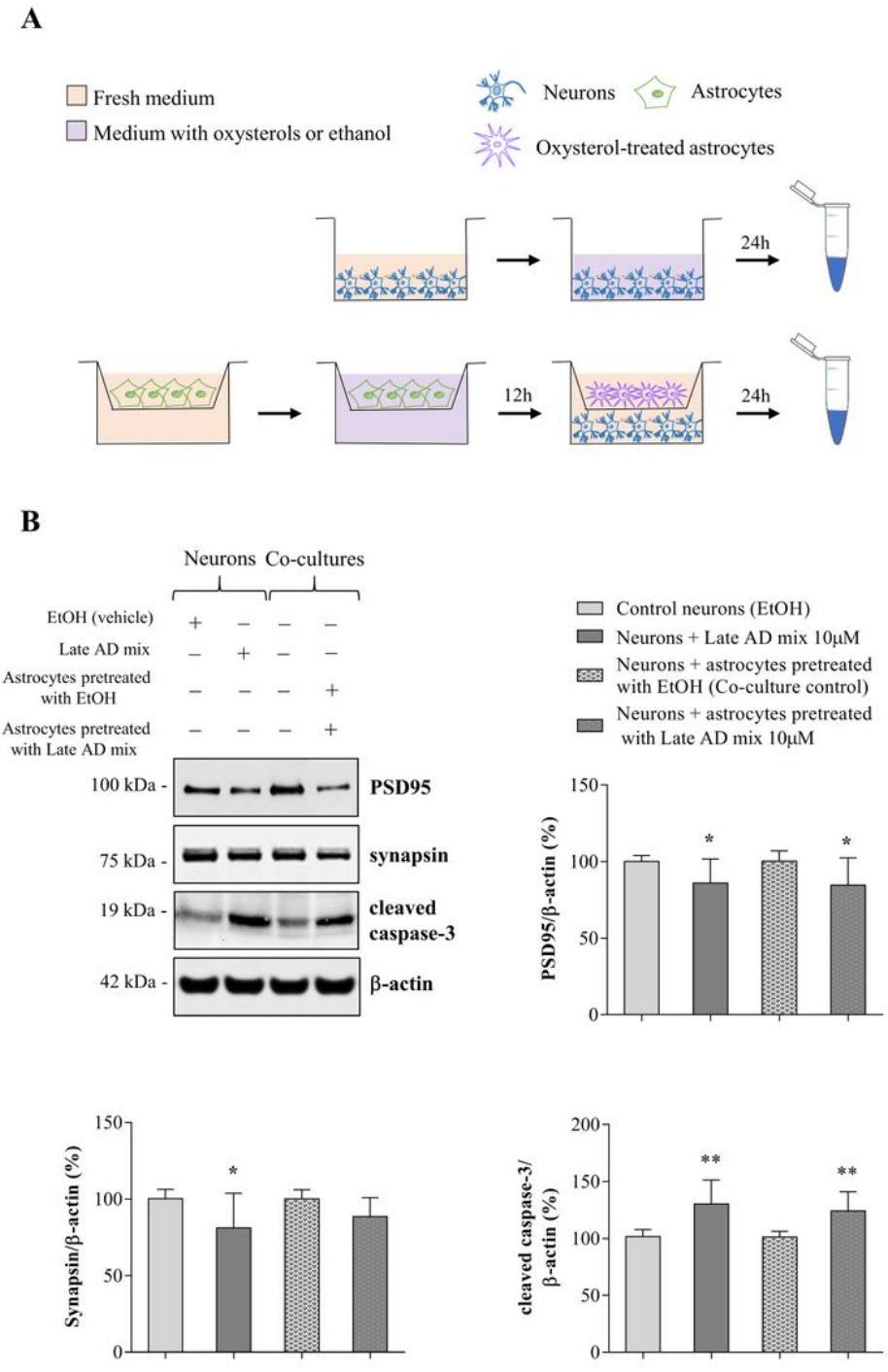

Figure 5

Oxysterol-stimulated astrocytes compromise neuronal health. Primary neurons (13 DIV) were treated with the Late AD oxysterol mixture (10 μM) for 24h or they were co-cultured for 24h with astrocytes grown on cell culture inserts that had been previously treated with the same oxysterol mixture for 12h. (A) Graphical representation of co-culture experiments. (B) The protein levels of the postsynaptic density protein 95 (PSD95), synapsin, and cleaved caspase-3 were determined by Western blotting. Data were normalized to

the corresponding β-actin levels. Data are expressed as mean values ± SD of three different experiments as percentage change from respective control (n=9, Student's t-test). **P<0.01 and *P<0.05 vs control.

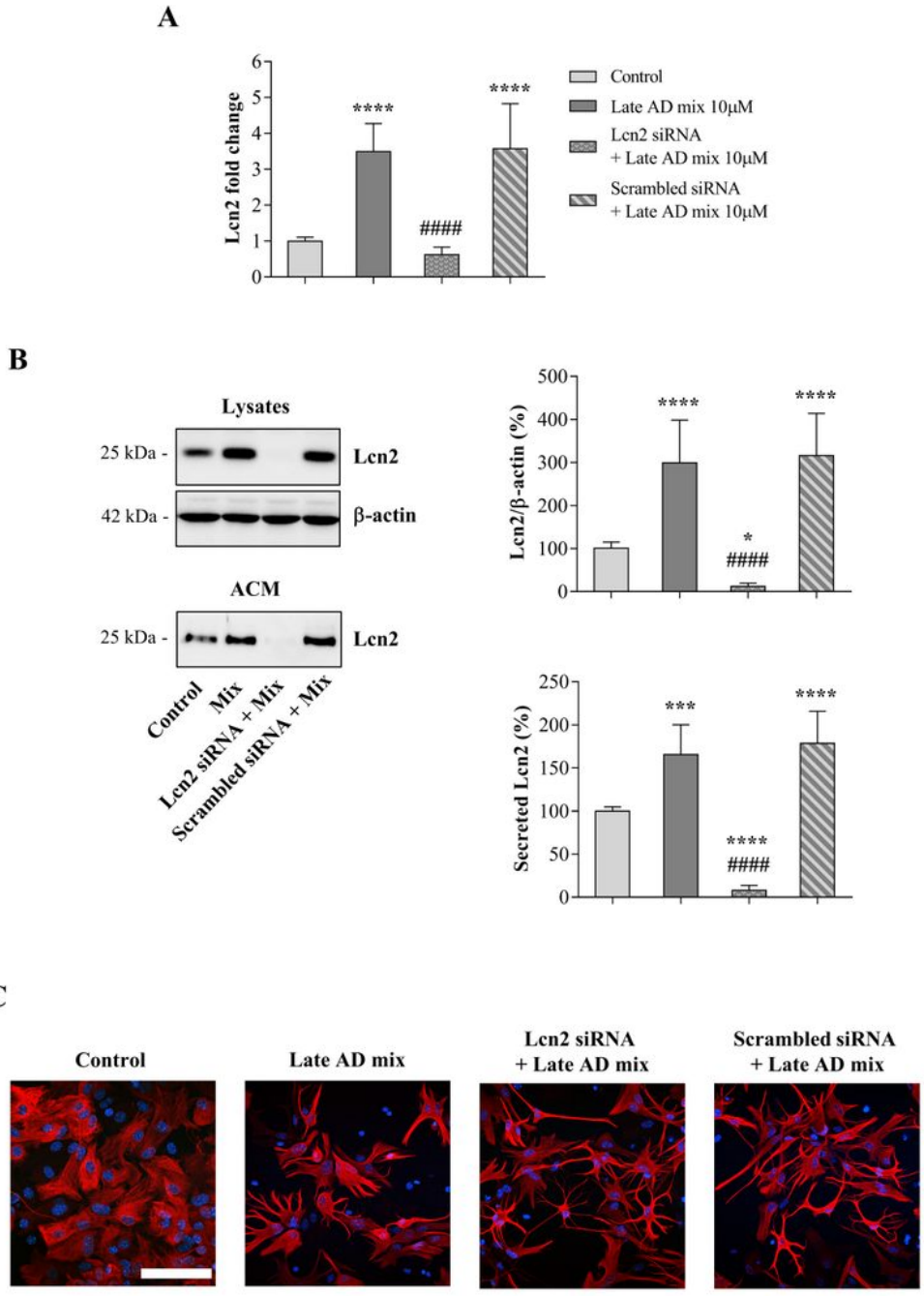

Figure 6

Lipocalin-2 (Lcn2) gene silencing prevents Lcn2 upregulation and release into the medium. Astrocyte cultures were transfected for 6h with Lcn2 or scrambled siRNA and then treated with the Late AD oxysterol mixture 10 μM (Mix) for 12h. After treatment, the medium was changed and astrocytes were

incubated with fresh medium for 24h. Transient Lcn2 gene knockdown was evaluated by (A) real-time RT-PCR and (B) Western blotting of both lysates and astrocyte conditioned media (ACM) samples. Data were normalized to the corresponding □-actin levels. Data are expressed as mean values ± SD from three different experiments as percentage change from control (n=9, one-way ANOVA). ****P<0.0001, ***P<0.001, and *P<0.05 vs control; #### P<0.0001 vs oxysterol treated. (C) Astrocyte morphology was examined by immunocytochemistry using a glial fibrillary acidic protein (GFAP) antibody (red) and nuclei were stained with Hoechst 33258 (blue). Representative images from three experiments are shown. Cells were imaged using an LSM800 confocal microscope (Zeiss, 40X objective; scale bar: 100 □m).

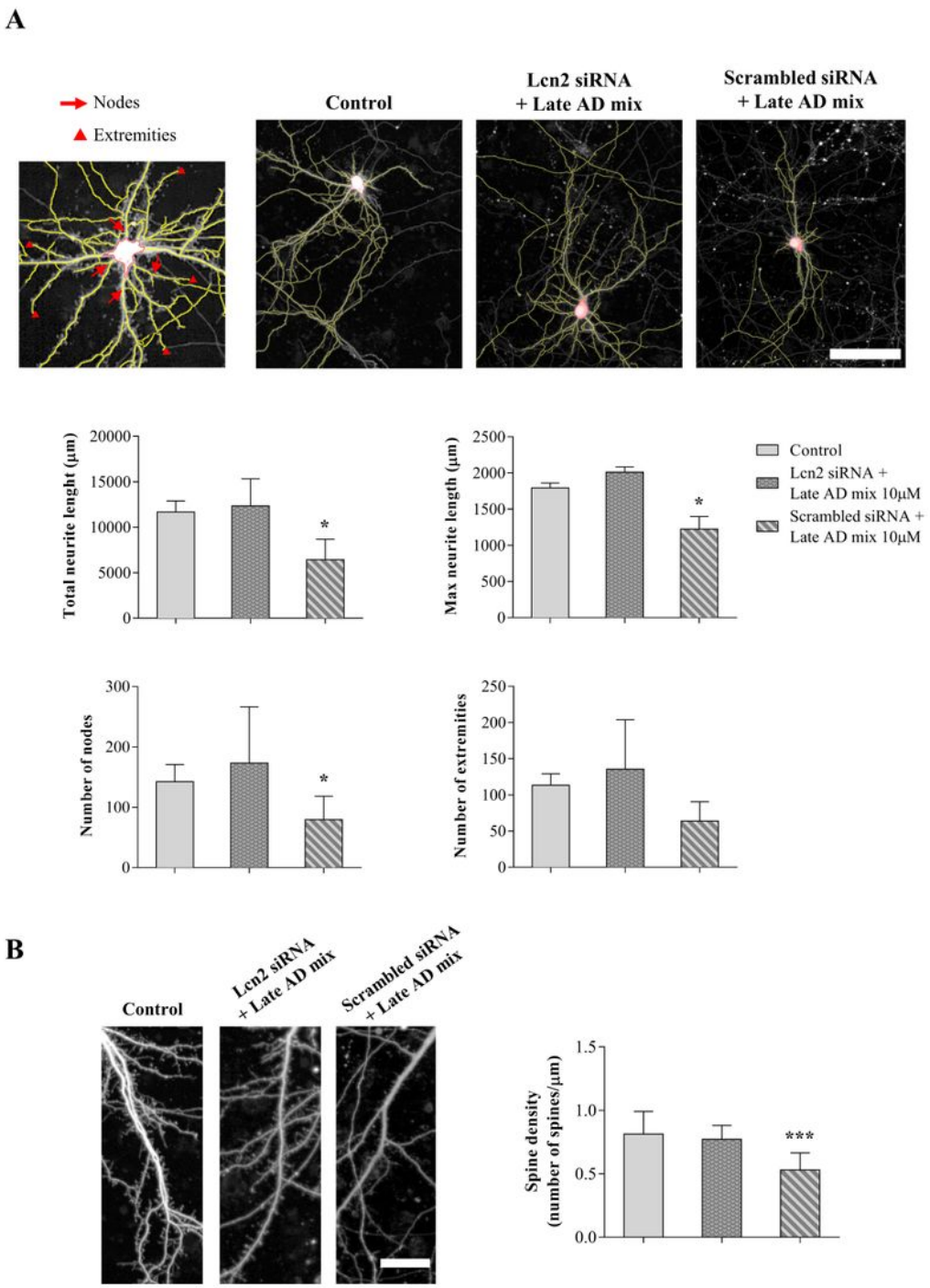

Figure 7

Lipocalin-2 (Lcn2) secreted by oxysterol-stimulated astrocytes affects neurite complexity and decreases dendritic spine density. Primary neurons were incubated for 24h with conditioned media from astrocytes transfected for 6h with Lcn2 or scrambled siRNA and then treated with the Late AD oxysterol mixture 10 M for 12h. After treatment, the medium was changed and astrocytes were incubated with fresh medium for 24h. High resolution digital images of live neurons were obtained using an Opera-Phenix microscope

(Perkin-Elmer). (A) Neurite complexity was analysed using Harmony software. Total and maximum neurite length, number of nodes and extremities were quantified and compared between groups. Representative images are shown (scale bar: 100 □m). Data are expressed as mean values ± SD from three different experiments and were obtained from analysis of 20 neurons/condition (one-way ANOVA). *P<0.05 vs control. (B) NeuronStudio software was used for dendritic spine analysis. Spine density was defined as number of spines per micrometer of dendrite length and was obtained from analysis of 20 neurons/condition (one-way ANOVA). Representative images are shown (scale bar: 25 □m). Data are expressed as mean values ± SD from three different experiments. ***P<0.001 vs control.

Supplementary Files

This is a list of supplementary files associated with this preprint. Click to download.

- SupplementalFig4.tif
- SupplementalFig3.tif
- SupplementalFig2.tif
- SupplementalFig1.tif